PROCESSING, STRUCTURE, AND TRIBOLOGICAL PROPERTY INTERRELATIONSHIPS IN SPUTTERED NANOCRYSTALLINE ZnO COATINGS

Wei-Lun Tu, B.S.

Thesis Prepared for the Degree of

MASTER OF SCIENCE

UNIVERSITY OF NORTH TEXAS

August 2009

APPROVED:

Thomas Scharf, Major Professor
Rajarshi Banerjee, Committee Member
Jincheng Du, Committee Member
Richard F. Reidy, Chair of the Department of Materials Science and Engineering
Costas Tsatsoulis, Dean of the College of Engineering
Michael Monticino, Dean of the Robert B. Toulouse School of Graduate Studies

Tu, Wei-Lun. Processing, Structure, and Tribological Property Interrelationships in Sputtered Nanocrystalline ZnO Coatings. Master of Science (Materials Science and Engineering), August 2009, 59 pp., 5 tables, 23 illustrations, references, 34 titles.

Solid lubricant coatings with controlled microstructures are good candidates in providing lubricity in moving mechanical assembly applications, such as orthopedics and bearing steels. Nanocrystalline ZnO coatings with a layered wurtzite crystal structure have the potential to function as a lubricious material by its defective structure which is controlled by sputter deposition. The interrelationships between sputtered ZnO, its nanocrystalline structure and its lubricity will be discussed in this thesis. The nanocrystalline ZnO coatings were deposited on silicon substrates and Ti alloys by RF magnetron sputtering with different substrate adhesion layers, direct current biases, and temperatures. X-ray diffraction identified that the ZnO (0002) preferred orientation was necessary to achieve low sliding friction and wear along with substrate biasing. In addition, other analyses such as scanning electron microscopy (SEM), transmission electron microscopy (TEM), and selected area electron diffraction (SAED) were utilized to study the solid lubrication mechanisms responsible for low friction and wear.

Copyright 2009

by

Wei-Lun Tu

ACKNOWLEDGEMENTS

I would like to present my deepest gratitude to my wonderful advisor, Dr. Thomas Scharf, who provided me with not only the knowledge which I needed for this work and the courses of my Masters degree but also the support for my life. His guidance, detailed explanations, and fabulous patience encouraged me to complete this work. I am really appreciative and glad to have him to be my advisor.

I also would like to give my acknowledgements to Drs. Raj Banerjee and Jincheng Du, who served as my research committee members and always offered me suggestions and support on this work. In addition, they also offered me teaching/research assistant positions. I need to thank Dr. David Diercks, Nancy Bunce, and Dr. Maia Castillo Romanes for their training and technical assistance with instrumentation throughout this research. Meanwhile, I would like to thank Dr. Junyeon Hawng and Dr. Somya Nag for their samples and analysis.

Lots of thanks goes to my friends and colleagues, especially Arun, Antariksh, Benedict, Hamid, Ming-Te, Fang-Ling, Ming-hang Li, Eric and others who made my stay here a one to remember.

Finally, I want to express my appreciation to my family, for their support throughout this academic journey. I would like to thank my parents; I couldn't complete this work and earn this degree without their full support. To my sister, who has always been my role model and encouraged me to pursue higher knowledge.

TABLE OF CONTENTS

Page

ACKNOWLEDGEMENTS iii

LIST OF TABLES vi

LIST OF FIGURES vii

Chapter

1. INTRODUCTION 1

1.1 Motivation 1

1.2 Contributions of Thesis 3

1.3 Organization of Thesis 3

2. OVERVIEW OF TRIBOLOGY, CERAMIC OXIDE SOLID LUBRICATION, AND PHYSICAL VAPOR DEPOSITION 5

2.1 Tribology 5

2.2 Oxide Ceramic Lubrication 6

2.2.1 Oxide Ceramics 6

2.2.2 Plastic Deformation in Nanocrystalline Oxide Materials 7

2.2.3 Lubricious Oxide Materials 8

2.3 Physical Vapor Deposition 10

2.3.1 Thin Film Physical Vapor Deposition Techniques 10

2.3.2 DC and RF Sputtering 11

2.3.3 Pulsed Laser Deposition 16

3. EXPERIMENTAL PROCEDURES 17

3.1 Preparation 17

3.1.1 Substrates (Silicon wafer, TNZT+2B, Ti64, CP-Ti) 17

3.1.2 Substrate Cleaning 18

3.2 Film Deposition 19

3.2.1 Deposition Conditions 19

3.2.2 Film Deposition by PVD 20

3.2.2.1 DC Magnetron Sputtering for Adhesion Layer.....21
3.2.2.2 RF Sputtering of Zinc Oxide Film.....22
3.2.3 Film Deposition by ALD.....22
3.2.4 Film Deposition by PLD.....23
3.3 Film Characterization.....23
3.3.1 Profilometer.....23
3.3.2 X-ray diffraction (XRD) and X-ray reflectivity (XRR).....23
3.3.3 Pin-on-Disc (POD) tribometer test.....24
3.3.4 Optical Microscopy.....25
3.3.5 Scanning Electron Microscopy.....25
3.3.6 Transmission Electron Microscopy.....25
4. RESULTS AND DISCUSSION.....26
4.1 Thin Film Condition Selection.....26
4.1.1 ZnO Thin Film on Si Wafer under Various Radio Frequency Power with No Bias at Room Temperature.....26
4.1.2 ZnO Thin Film on Si Wafer under 200W Radio Frequency Power with Various Conditions.....31
4.2 ZnO Coatings Deposited on Ti-Alloys.....40
4.2.1 The Structure of ZnO Films on Ti Alloys.....41
4.2.2 Wear Behavior of ZnO Coated and Uncoated Ti Alloys.....43
4.2.3 Wear Behavior Comparison of Different Deposition Techniques.....45
5. Conclusions.....54
BIBLIOGRAPHY.....56

LIST OF TABLES

Page

1. Deposition conditions and thin film designation of magnetron sputtering (substrate at room temperature). 20
2. Deposition conditions and thin film designation of magnetron sputtering (substrate heated to 400C). 20
3. The pin on disc test design setting. 25
4. The GIXRD reflection peaks and corresponding μ_{ss} values of the ZnO films with Nb adhesion layer under varying deposition conditions. 31
5. The GIXRD reflection peaks and corresponding μ_{ss} values of the ZnO films with Ti adhesion layer under varying deposition conditions. 32

LIST OF FIGURES

Page

1. ZnO structure (wurtzite structure). 10
2. The schematic diagram of DC sputtering system. 13
3. The schematic diagram of RF sputtering system. 14
4. (a) The schematic diagram of bias sputtering (DC power source) system. (b) Effect of plasma with and without bias sputtering. 15
5. Substrate Cleaning Procedure. 19
6. Photo of Kurt J. Lesker PVD-75 sputtering system for ZnO thin film depositions. 21
7. Photo of Savannah 100 ALD system for ZnO thin film depositions. 22
8. Photo of Lambda Physik Compe201 pulsed laser deposition system for ZnO thin film depositions. 23
9. GIXRD spectra of ZnO films as a function of RF power (a), deposition rate and grain size of ZnO films (b). The figures show that the intensity of (0002) peak, deposition rate, and grain sizes of the films all increasing RF power. 27
10. Optical microscope photos of zinc oxide thin films after POD tribometer testing. RF sputtering power: (a) 50W, (b) 100W, and (c) 200W. 30
11. The XRR spectra of the ZnO film deposited (a) with -50V substrate bias, and (b) without bias. 34
12. XRD spectra of ZnO films as a function of bias voltage: (a) bias 0V, (b) bias -25V, (c) bias -50V, (d) bias -75V, and (e) bias -100V. 37
13. Comparison between wear factors of ZnO films on Nb and Ti adhesion layers. 39
14. Comparison of wear factors of ZnO films on Nb adhesion layer as a function of various deposition conditions. The film deposited at 400C with - 50V bias has the lowest wear factor. 40
15. XRD spectrum of ZnO film sputtered on Ti alloy, TNZT+2B. 41
16. XRD spectrum of ZnO film sputtered on Ti alloy, Ti-6Al-4V. 42
17. XRD spectrum of ZnO film sputtered on Ti alloy, CP-Ti. 42
18. Optical microscope wear track images of uncoated Ti alloys and sputtered ZnO coated Ti alloys, (a) uncoated CP-Ti and sputtered ZnO on CP-Ti, (b) uncoated Ti-6Al-4V and

sputtered ZnO on Ti-6Al-4V, (c) uncoated TNZT+2B and sputtered ZnO on TNZT+2B. 44
19. Wear factors of ZnO coated and uncoated Ti-alloys. 45
20. ZnO wear factors comparing different deposition techniques sputtering (PVD technique), atomic layer deposition (CVD technique), and pulsed laser deposition (PVD technique). 46
21. HRSEM image of ZnO wear track on TNZT+2B showing location of cross-sectional FIB-cut. Inset image shows a low magnification XTEM image of the FIB-cut displaying the sputtered layers. 47
22. (a) XTEM image of ZnO outside the wear track (unworn). The interfaces of the sputtered layers and TNZT+2B substrate are clearly shown. Image shows nano-columnar grains (smaller near bottom) with no texture near surface. (b) Corresponding indexed electron diffraction pattern (FFT image) of single ZnO nano-columnar grain near the surface looking down the zone axis, z=[1-21-3] 49
23. (a) XTEM image of FIB-cut shown in Figure 4-13 for ZnO inside the wear track (worn). The interfaces of the sputtered layers and TNZT+2B substrate are clearly shown. Image shows that the grains underwent considerable deformation (denoted by orange arrows) in addition to the smoothing of the surface. (b) Corresponding indexed electron diffraction pattern (FFT image) of single ZnO nano-columnar grain near the surface looking down the zone axis, z=[1-21-3]. Blue arrows show additional diffraction spots indicative of multiple, finer scale grains with local rotation due to the tribological stress/strain-induced sliding process. 51

CHAPTER 1

INTRODUCTION

1.1 Motivation

After a long term evaluation of technology, humans are able to remedy diseases that could not be cured previously; therefore, humans have the ability to extend their lives. However, complications due to ageing will be one serious problem if people have longer lives. Ageing not only affect organs but also bones. With people getting older, part of bone in load bearing joints, e.g., the hip joint, could be worn off or damaged by the long term use or accident impact. Presently, the normal treatment is for implants to replace surgery of the bones. Therefore, if the average age of population is increased in the world, i.e., the population is getting old, more and better quality of implants are required. In implant surgery, the designed implant will replace the body's natural materials, and thus they must be biomaterials, i.e., biocompatibility with the body.[1] In addition, most of the current implants are metallic alloys, which exhibit high elastic modulus (stiffness), so the next generation of biomaterials need to exhibit lower elastic modulus (compliant) to be comparable with bone and thus prevent stress shielding. Also, the materials used to replace the bones must support the weight and strength of the body, so they need high strength to be good implant materials. Currently, titanium alloys are able to satisfy this last requirement, so most implant materials in load bearing joints are composed of titanium alloys. However, the previously mentioned stress shielding issue is a problem, as well as the poor wear resistance of titanium alloys. This poor wear resistance will generate harmful metallic wear debris that can enter into the blood stream. Accordingly, better implant materials which have low friction and thereby good wear resistance are necessary.

Normally solid, large grain oxide materials, like zinc oxide, are brittle and exhibit high

friction and wear. However, in a study[2] by Zabinski et al., it was reported that thin film nanocrystalline grain size zinc oxide has high potential to be a lubricious material because it is relatively soft, ductile and the chemical stoichiometry and microstructure can be controlled to introduce defects into the film, which are all controlled by the deposition process. In addition, oxides can contribute to environmental and thermal stability in moist and oxidizing environments, respectively. In studies[3,4] by Gleiter et al., it was reported that once the grain size of oxides can be reduced down to a few nanometers, which will allow nanoscale zinc oxide to plastically deform and become ductile in contrast to conventional microcrystalline oxide ceramics that elastically deform and are inherently brittle. In another study[5], it was also mentioned that nanocrystalline metals can deform plastically due to a grain boundary sliding mechanism. Therefore, the motivation behind this thesis is to determine if a bias sputtering process can control the grain size and defects in zinc oxide solid lubricant thin films/coatings and if the structure can allow for low friction and long wear life. In addition, the main focus of this thesis was to determine the experimental sputtering conditions to achieve these nanoscale zinc oxide coatings on various titanium alloys and test their friction and wear (tribological) properties.

Physical vapor deposition (PVD) techniques, like bias sputtering, have found widespread use in many industrial sectors. These techniques allow for the deposition of metals, alloys, ceramics, and polymer thin films onto a wide range of substrate materials. The physical vapor deposition is also a proven method to deposit zinc oxide thin films in many studies[6-9]. There are many experimental parameters, such as pressure, power of source target, substrate temperature, substrate bias, etc. used in physical vapor deposition that will affect the properties of zinc oxide thin films. The deposition conditions to achieve low friction and good wear resistance in nanoscale zinc oxide thin films will be one of the main goals of this thesis. Pin on disc tribological testing will be used to

measure and select the best friction and wear behavior of zinc oxide thin films. In this type of test, a stainless steel ball is the pin material in direct contact with the disc which is sputtered zinc oxide deposited on titanium alloy substrates. The coefficient of friction (COF) and the wear factor of the zinc oxide thin films and the uncoated substrates will be measured by the pin on disc tribometer. For example, to be shown later in this thesis, the wear factor of bare titanium alloys is approximately 10^{-3} mm^3/Nm, and it decreases to less than 10^{-6} mm^3/Nm after coating the titanium substrates with zinc oxide. Based on the presented results, it is the hope that these coated materials can be a better alternative to currently used implant materials.

1.2 Contributions of Thesis

(A). Investigate a deposition method and experimental conditions to synthesize a lubricious coating to improve the wear resistance of titanium alloys, and thereby extending the life of implant materials.

(B). Determine how the sputter deposition parameters control the nanocrystalline zinc oxide grain growth, orientation and density.

(C). Investigate the plastic deformation mechanisms of nanocrystalline zinc oxide thin films during tribological sliding. Comparisons will be made between the deformation mechanisms with bulk zinc oxide.

(D). Confirm how the ZnO nanocrystalline (0002) texture is able to help the coatings form lubricious surface and subsurfaces by reorientation and plastic deformation.

1.3 Organization of Thesis

There are five chapters in the thesis. This chapter just presented the introduction and motivation of the research. Chapter 2 presents an overview of tribology, solid lubrication mechanisms of nanocrystalline solid oxides, and physical vapor deposition technique used to

sputter the zinc oxide thin films. This chapter also gives the theory of tribometer testing to describe the measurement of the friction and wear factor. Chapter 3 provides experimental details which include the sputter deposition process conditions and characterization techniques used to study the films. Chapter 4 is the results and discussion based on the preceding experiments. Chapter 5, the last, is the conclusions and future work.

CHAPTER 2

OVERVIEW OF TRIBOLOGY, CERAMIC OXIDE SOLID LUBRICATION, AND PHYSICAL VAPOR DEPOSITION

2.1 Tribology

Tribology is the science and technology of interacting surfaces in relative motion. It includes the study and application of the principles of friction, lubrication and wear. The friction is the force resisting the related motion of two surfaces. The frictional force, F_f, is related to the force or weight acting normal to the direction of motion (F_n) by the coefficient of friction (COF) and that can be written into a formula: $COF= F_f/F_n$. The coefficient of friction, and other tribological characteristics, is a function of the nature of the contact force, velocity, interacting surfaces, environment, temperature, and other factors, which in other words, makes it a system's property and not a material's property. According to the Bowden-Tabor model of friction, the interfacial shear stress, τ, of the surfaces at the location of contact is related to the frictional force, so that the interfacial shear stress, $\tau= F_f/A_r$, where A_r is the real area of contact in the interface. Therefore, one can rewrite the coefficient of friction formula, $COF= \tau A_r/F_n$, this formula tells us that COF increases when the real area of contact is increasing. The real area of contact is a function of the interface loading conditions, surface topography and material properties and thus is difficult to determine experimentally. Based on this, during the test I maintain the same normal load so the stress will be constant, assuming the contact area does not change, e.g. ball wear, and thus I graph the COF versus distance to determine the tribological behavior of the film.

2.2 Oxide Ceramic Lubrication

2.2.1 Oxide Ceramics

The reaction of metal with oxygen will form oxide ceramics materials. Correlated to the difference in electronegativities (EN) between oxygen and metals, generally oxide ceramics have covalent (similar EN), ionic (large difference in EN) or mixed bonds. Ionic/covalent bonds tend to have large bond/lattice energies, so the high strength, hardness, chemical and thermal resistance will become the properties of these materials. They are the first rate materials for demanding applications which require these characteristics. However, because these bonds are strong and it is difficult for dislocations to move to cause crystalline slip in microcrystalline ceramics, these materials exhibit brittle fracture at low temperatures. The brittle fracture is the typical failure model in oxide ceramics. This happens when a critical stress is reached at a weak point (flaw) in the oxide ceramic and a crack initiates and rapidly propagates throughout the material causing failure. Most oxide ceramics have numerous preexisting defects/flaws or invisible cracks. Little or no ductile deformation occurs in the surrounding areas of the crack. When used in interacting or sliding surfaces, progressive crack generation in oxide ceramics results in the formation of large wear particles that are abrasive to both contacting surfaces. This results in high friction and significant wear by a third body abrasive wear mechanism, which eventually leads to device or equipment failure. In addition, oxide ceramics at ambient temperatures have low fracture toughness properties. However, recent studies have determined that in the nanoscale grain size regime, ceramics can plastically deform at ambient temperature.[10] As a result, they potentially have use in demanding tribological applications such as mechanical seals, prosthetic devices and ball bearings as well as becoming reliable materials for a wide range of applications in extreme conditions. The bulk oxides normally have crystal grain sizes of more than 1 micron (10^{-6}m). The

plastic deformation which is caused by slip in bulk oxide ceramics does not exist or only to a very limited extent due to large Burgers vector (unit of slip) distances and ions of like charge resist motion (repulsion). Also, the cracks of bulk oxide ceramic materials are normally sharp at the atomic level[11]. As a result; the debris is sharp and very abrasive to the wear behavior of bulk oxide ceramics. A review study of bulk oxide ceramics wear behavior is presented by Rainforth[12]. In the study; he classified wear in oxide ceramics as being mild or severe. The transition of wear behavior between mild and severe regime has been studied in order for its prevention[13]. To increase the resistance to fracture in oxide ceramics there has been studies aimed at modifying the material's microstructure. Rainforth has identified and discussed three strategies for modifying oxide ceramics microstructure in order to increase the fracture resistance. One of the strategies is general reduction in the microstructural scale specifically that of grain size and porosity. This strategy based on the nanocrystalline oxide film may generate smooth surfaces and prevent fracture, and thus increase the oxide's wear resistance.

2.2.2 Plastic Deformation in Nanocrystalline Oxide Materials

Plastic deformation is an irreversible process where deformation will existed even after the force or stress is removed. Normally the plastic deformation is combined with slip which is the process by which dislocations move within a crystalline material along close-packed planes and directions. Most oxide ceramics have limited number of slip system and it's hard to activate them without thermal processes. Therefore, plastic deformation is rarely observed in oxide ceramics at room temperature[14]. It's a significant advantage for oxide ceramics in engineering applications that plastically deform to create low-friction and long-life coatings. Gleiter and his colleagues[15] have reported that conventional brittle polycrystalline ceramics could become ductile if their grain size is reduced to a few nanometers. In addition, Schiotz and coworkers[16] used computer

simulations to demonstrate the plastic deformation in nanocrystalline metals could be achieved mainly by grain boundary sliding and a minor contribution from dislocation activity in the grains. Their research proposed the Inverse Hall-Petch effect in which deformation happens along nanocrystalline grain boundaries in contrast to the normal Hall-Petch where deformation classically occurs by slip and yield stress. In the normal Hall-Petch regime the finer grain size (above 1 micron not approached at the nanoscale) has greater total grain boundary area to stop dislocation slip thereby increasing the strength of the material. Once the grain size of materials are reduced to the nanoscale, then these materials may deform by an inverse Hall-Petch phenomena in which there is grain boundary activity. Thus, finer grained materials would be softer and more deformable. This theory, which is under current debate, states that there exists a critical grain size (cross-over grain size) which defines the deformation mechanism by changing from dislocation motion to grain boundary processes. In addition, their theory states that normal brittle polycrystalline materials could become ductile if their grain size is reduced to a few nanometers. This phenomenon becomes a major motivation factor in this thesis to promote ductility and plasticity in nanocrystalline oxide coatings during tribological contact.

2.2.3 Lubricious Oxide Materials

Traditionally, most bulk, large grain size oxides are normally brittle and have high friction which generates large amounts of wear debris. Their brittleness and inability to plastically deform is because dislocation motion is difficult since ions of like charge resist motion through repulsion and Burgers vector (unit of slip) distances are large. However, in 2000, Zabinski and coworkers[17] determined that nanocrystalline zinc oxide thin films grown by pulsed laser deposition (PLD) can be made ductile by controlling their microstructure. Zinc oxide (ZnO) typically has the wurtzite crystal structure (space group $P6_3mc$) which is based on a hexagonal Bravais lattice (a=0.324 nm

and *c*=0.519 nm). Fig.2-1 shows the wurtzite crystal structure of ZnO. In Zabinski's ZnO deposition, it was found that highly defective nanocrystalline columnar grains that had sub-grains within can result in low friction and long wear at room temperature. The ZnO has multiple thermodynamically stable faces like (0001) and (10-10) which have different surface energies and mechanical properties. In the Henrich report, (0001)-orientated grains have the lowest surface energy, and this highly lubricious orientation of ZnO is controlled by the film's deposition conditions.[18] They proposed the (0001) texture of ZnO has nano-columnar microstructure which can be repeated by controlling the microstructure and chemical properties to be a good lubricious material in tribology at ambient temperature.

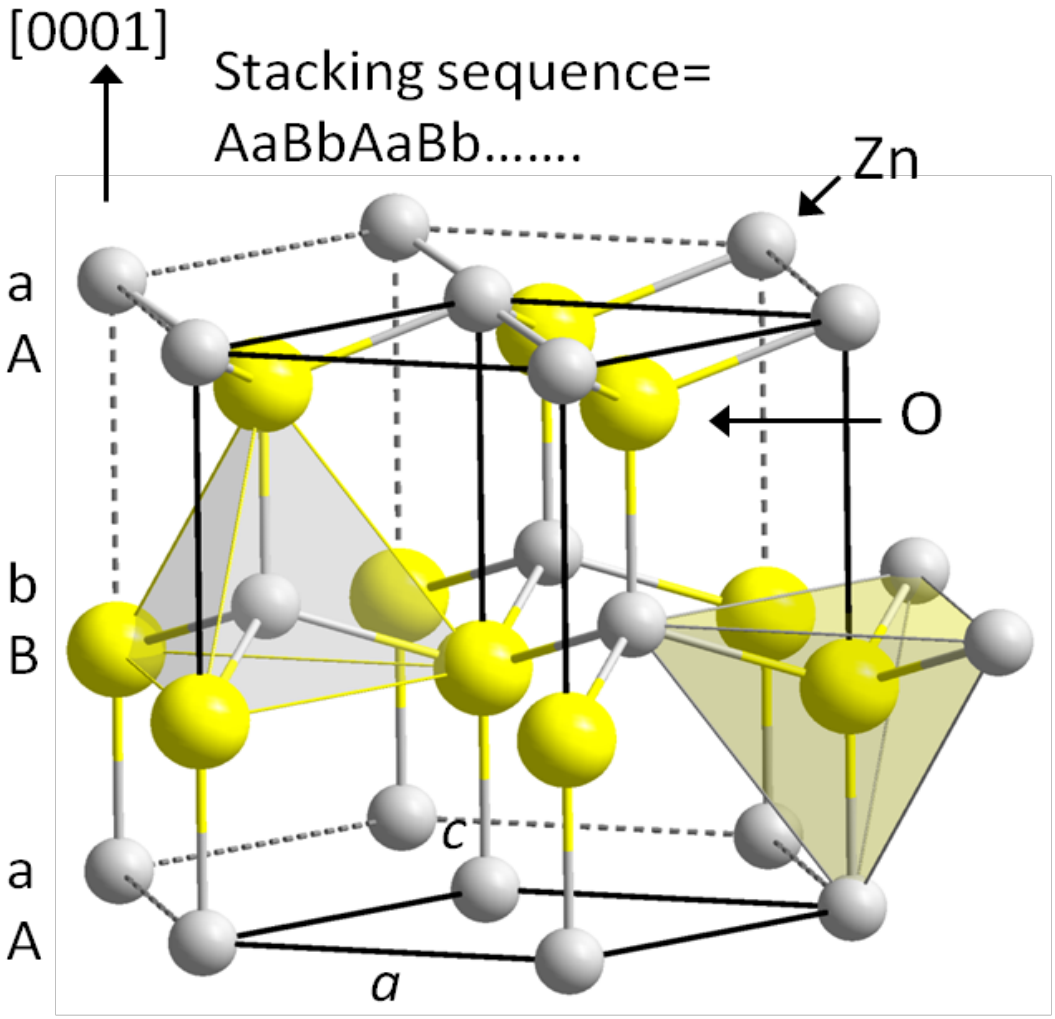

Figure 2-1: ZnO structure (wurtzite structure).

2.3 Physical Vapor Deposition

2.3.1 Thin Film Physical Vapor Deposition Techniques

"Deposition of thin films by physical vapor deposition (PVD) techniques has found widespread use in many industrial sectors. The PVD processes allow for the deposition of metals, alloys, ceramics, and polymer thin films onto a wide range of substrate materials".[19] There are many methods of depositing PVD coatings, including magnetron sputtering, arc evaporation and the aforementioned PLD. In this research, we focused on radio frequency (RF) and direct current

(DC) magnetron sputtering with substrate biasing to grow zinc oxide thin films for improved surface engineering and solid lubrication applications such as coating titanium orthopedic implants and high temperature aerospace solid lubricants, respectively. The PLD technique was also used in this thesis to deposit zinc oxide control samples to compare to sputtering and other deposition processes.[19]

2.3.2 DC and RF Sputtering

"Sputtering is a vacuum process used to deposit very thin films on substrates for a wide variety of commercial and scientific purposes. It is performed by applying a high voltage across a low-pressure gas to create plasma which consists of electrons and gas ions in a high-energy state".[20] In some other studies the process is referred to as glow discharge, which gives off a colored aura of light from the plasma. "During sputtering, the energized plasma ions strike on a material target (usually ~99.99% pure) which is composed of the desired coating material, and cause atoms from that target to be ejected with enough energy to travel to, and bond with, the substrate"[20] and by nucleation and growth deposit a thin film. However, the plasma ions are transferred between the target and substrate with high energy, and if without a method controlling it to direct the flow of atoms in the processes, then sputtering cannot be a practical way for mass production. As a result, in order to fix the glow discharge problem, the "planar magnetron" was discovered to solve this problem in the 1960s. "This technology uses powerful magnets to confine the "glow discharge" plasma to the region closest to the target plate. This vastly improves the deposition rate by maintaining a higher density of ions, which makes the electron and gas molecule collision process much more efficient".[20] Presently, with the help of strong magnets, magnetron sputtering is a more powerful and flexible technique which can be used to coat virtually any specimen with a wide range of materials, including metals/alloys and a variety of ceramics. In

addition, because the energetic ions are able to move in curved directions that increase the range of sputtering area, magnetron sputtering can provide smooth depositional thin films.[21] Otherwise, the ions affected by the magnetron field can move in a curved way, so they can increase the rate of ion collisions which can enhance the ability to ionize the material and thus help improve the structure and properties of the thin film. In general, according to the difference in power source, magnetron sputtering can be divided into three types: radio frequency (RF) magnetron sputtering, direct current (DC) magnetron sputtering, and medium frequency-pulse Direct Current magnetron sputtering (MF-pulse DC). In this thesis, RF magnetron sputtering of a ZnO insulator target was used to deposit ZnO thin films with dc substrate biasing, and DC magnetron sputtering with conductive target, niobium or titanium, was used to deposit an adhesion layer on various substrate materials.

A. Direct Current (DC) Magnetron Sputtering

"Direct current magnetron sputtering is a widely used technique for deposition of metal and compound layers for numerous technical applications. It is a plasma technique utilizing magnetic fields to enhance and confine the plasma close to the deposition source. The deposition species are vaporized by sputtering from the target by ion bombardment".[19] In this thesis, DC magnetron sputtering was used to deposit an adhesion layer, Nb or Ti, to the substrate. Fig. 2-2 shows the schematic of direct current magnetron sputtering system.

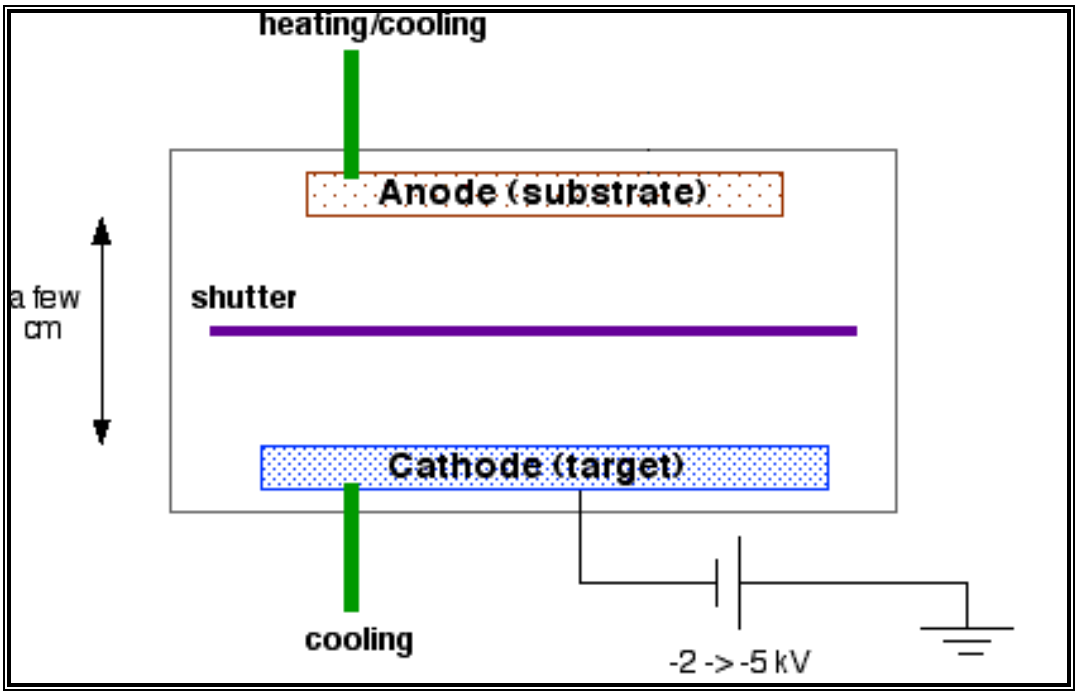

Figure 2-2: The schematic diagram of DC sputtering system.

B. Radio Frequency (RF) Magnetron Sputtering

Radio frequency magnetron sputtering is good for depositing electrically insulating materials.[22] In the DC system, positive charge builds up on the target - it needs 1012 volts to sputter insulators. This is ineffective to apply so much high power during sputtering. Therefore, radio frequency was used instead of direct current power to sputter oxide layers, e.g., zinc oxide. The additional advantages to operate radio frequency power are ease of use to keep plasma going under particular conditions and ability to operate at lower working gas pressures. Fig. 2-3 shows the basic schematic of radio frequency magnetron sputtering system.

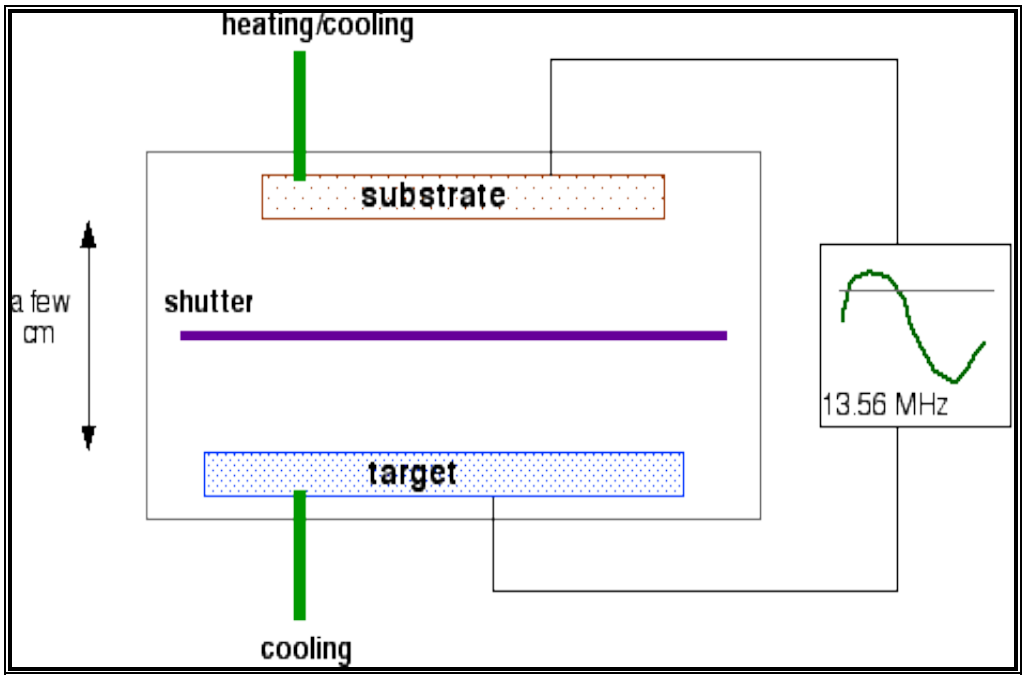

Figure 2-3: The schematic diagram of RF sputtering system.

C. Substrate biasing application

In 1962, Wehner[22] used bias sputtering to improve the epitaxial growth of silicon films on germanium substrates. Fig. 2-4 presents the basic setup of bias sputtering. Bias sputtering allows the voltage of the substrates to be adjusted relative to the growing film. Therefore, bias sputtering is able to enhance the ion impact energy which increases the deposition rate, the interfacial density, and the density of the sputtered layer(s). As a result, bias sputtering can increase the thin film density close to the material's theoretical value. Denser films usually lead to better material properties. The film's density can be measured by x-ray reflectivity (XRR) as will be shown in Chapter 4.

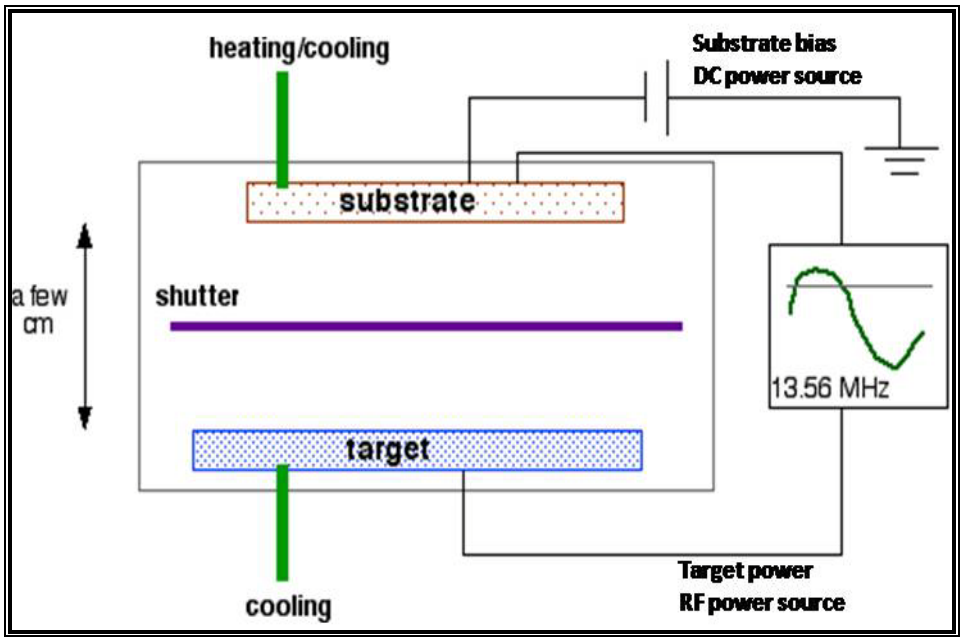

(a)

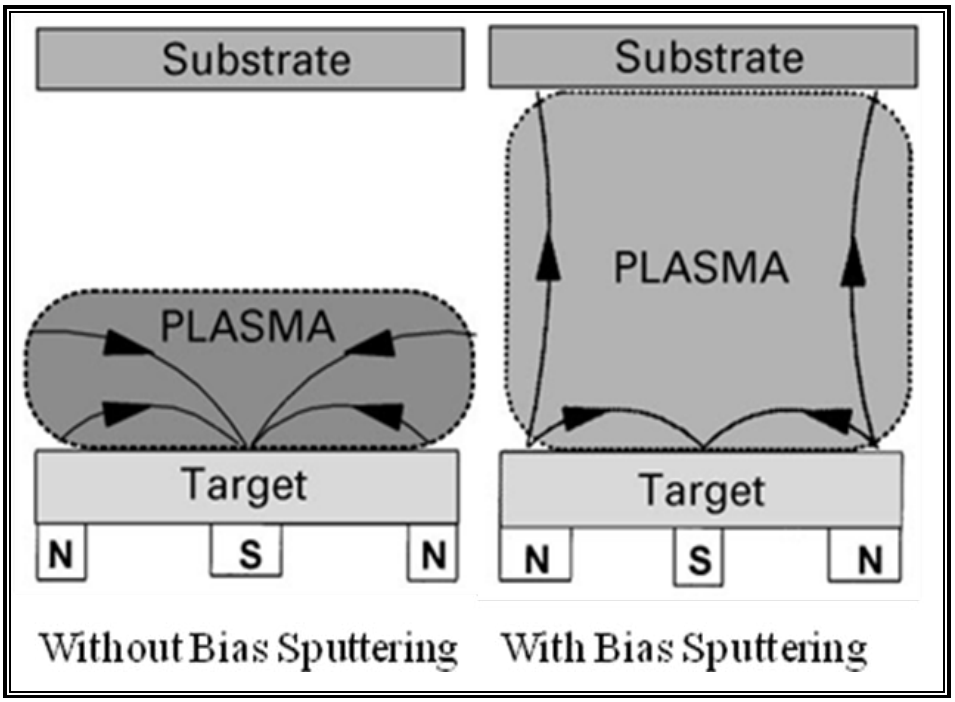

(b)

Figure 2-4: (a) The schematic diagram of bias sputtering (DC power source) system. (b) Effect of plasma with and without bias sputtering.

2.3.3 Pulsed Laser Deposition

The idea of PLD is that a pulsed laser beam is focused onto the surface of a solid target which is the material to be deposited. The powerful absorption of the electromagnetic radiation by the target causes evaporation of the target materials. The evaporated materials contain lots of excited and ionized species. This plasma plume will form in front of the target external if the ablation is carried out in the vacuum chamber. The plasma plume is the evaporated materials themselves. In the PLD process, some parameters need to be controlled like laser energy density and pulse repetition rate. The advantages of PLD are that the size of deposition targets is smaller than those used in other techniques like sputtering. In addition, PLD can use many different materials to deposit multi-layered films by continuous ablation of different targets. Another advantage is the ability to produce a fine control of film thickness down to atomic monolayer by controlling the frequency of pulses. Lastly, and the most important feature is PLD is able to retain the stoichiometry of the target in the deposited films. In this thesis, sputtering and PLD were used to deposit solid lubricant ZnO films, study their microstructure and how it determines tribological properties such as friction coefficient and wear rate.

CHAPTER 3

EXPERIMENTAL PROCEDURES

In this chapter, all of the experimental equipment will be described that was used to produce the thin film layers as well as the characterization of them. The equipment belongs to UNT's Department of Materials Science and Engineering (UNT MSE) and Center for Advanced Research and Technology (CART).

3.1 Preparation

3.1.1 Substrates (Silicon wafer, TNZT+2B, Ti64, CP-Ti)

Currently the stem material in hip implants is made of Ti-alloys, which have important properties such as good antirust, high strength, and good mechanical hardness. However, better biomaterials are needed for orthopedic implants for the following reasons. First, currently used titanium alloys have elastic modulus mismatch with bone (>110 GPa versus 28 GPa) that will lead to stress-shielding and long-term problems such as the bone resorption and osteoporosis, which means alternative materials are needed that exhibit low modulus and high strength to solve these problems. Second, there are biocompatibility issues with alloying additions, V and Al, to titanium that recent studies[24,25] report will have a toxic effect to the body. Lastly, there is inadequate wear resistance of the load bearing surfaces and there is a need for better adhesion to and growth of bone tissue. Based on these issues, there have been studies using the laser engineered net shaping (LENS^{TM}) process to add tough borides into Ti alloys to grow titanium-niobium-zirconium-tantalum + TiB precipitate (TNZT+2B) composites, which exhibit lower modulus (50GPa) and higher strength than currently used orthopedic implant materials[26].In this thesis, nanocrystalline zinc oxide thin films/coatings were grown on the surface of various titanium alloys by physical vapor deposition (PVD) methods bias sputtering and pulsed laser

deposition (PLD) to mitigate friction and wear in the base titanium alloys. The three Ti-alloys selected are TNZT+2B, Ti-6Al-4V, and commercially pure (CP)-Ti; the latter two materials are currently used to make orthopedic implant stems. The TNZT+2B alloy was previously deposited from LENS^{TM} processing by Dr. Souyma Nag of the Ohio State University. Each Ti alloy has ~15mm diameter and ~2-3mm thickness. Furthermore, for baseline studies to determine the zinc oxide (ZnO) coating experimental parameters resulting in best tribological performance, the coatings were deposited on single crystal (100) or (111)-orientated silicon wafers.

3.1.2 Substrate Cleaning

The following procedure was used to clean the substrates before they were loaded into the sputtering chamber. First, acetone was used with sonication for 5 minutes to clean the organic particles on the surface of substrate. This was followed by rinsing with deionized water and then sonicating with methanol for another 5 minutes to further clean the substrates. Finally, after sonicating with deionized water for 5 minutes, the substrates were blown dry with high purity nitrogen gas. Fig.3-1 summarizes the cleaning procedure.

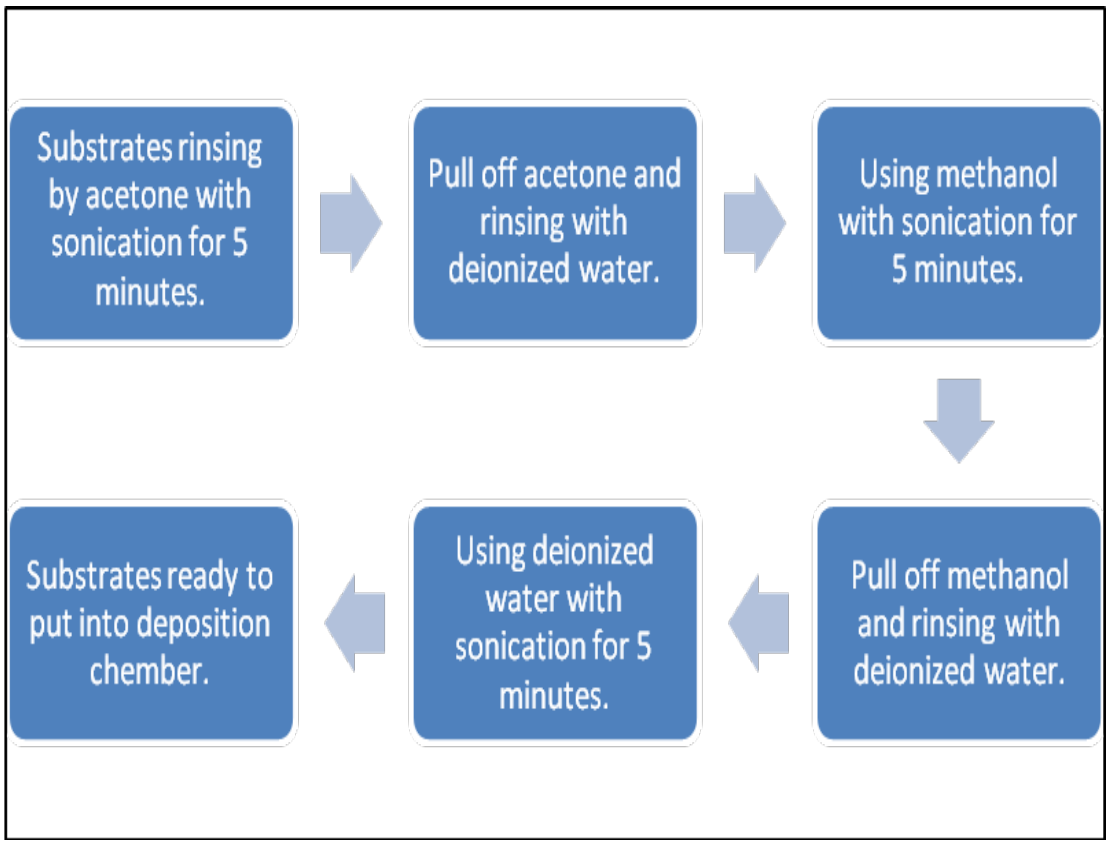

Figure 3-1: Substrate Cleaning Procedure.

3.2 Film Deposition

3.2.1 Deposition Conditions

Table 3-1 and 3-2 show the sputter deposition conditions. According to other studies[27-29] of zinc oxide thin films, sputtering parameters such as plasma excitation, working pressure, substrate bias, working distance, and substrate heating could significantly change the quality and microstructure of the films. In this thesis, various sputtering parameters were investigated such as target power, substrate temperature and bias. These parameters will be shown to affect ZnO structure, the coefficient of friction (COF), and wear rate. In addition, atomic layer deposition (ALD) and pulsed laser deposition (PLD) techniques were used for comparative purposes.

Adhesion layer	Nb / Ti	50W of RF target power	100W of RF target power	200W of RF target power
No Bias on substrate		A1	A2	A3
		a1	a2	a3
Negative 50V bias on substrate		B1	B2	B3
		b1	b2	b3
Negative 100V bias on substrate		C1	C2	C3
		c1	c2	c3

Table 3-1: Deposition conditions and thin film designation of magnetron sputtering (substrate at room temperature).

Adhesion layer	Nb / Ti	50W of RF target power	100W of RF target power	200W of RF target power
No Bias on substrate		D1	D2	D3
		d1	d2	d3
Negative 50V bias on substrate		E1	E2	E3
		e1	e2	e3
Negative 100V bias on substrate		F1	F2	F3
		f1	f2	f3

Table 3-2: Deposition conditions and thin film designation of magnetron sputtering (substrate heated to 400C).

3.2.2 Film Deposition by PVD

After the previously mentioned procedure for substrate cleaning, a Kurt J. Lesker PVD-75 system, Fig. 3-2, was used for ZnO sputtering. The chamber was pumped down overnight to reach around $5x10^{-7}$ Torr base pressure. Pure argon gas was introduced into the chamber at a working pressure of 5 mTorr. An ~80 nm thick adhesion layer (Nb or Ti) was first direct current (DC) magnetron sputtered onto the substrates at a power of 200W for 8 minutes. This was followed by radio frequency (RF) magnetron sputtering of an ~ 500 nm thick ZnO film under various sputtering powers from 50 to 200W. The varying power was chosen to study the effects of grain orientation (textured versus randomly oriented) on the tribological properties. In

addition, substrate temperatures (room temperature vs. 400C) and bias voltages (-50 to – 100V) were varied to study similar effects of structure on properties.

Figure 3-2: Photo of Kurt J. Lesker PVD-75 sputtering system for ZnO thin film depositions.

3.2.2.1 DC Magnetron Sputtering for Adhesion Layer

Between the substrate and the ZnO film, an adhesion layer was deposited to reduce the thermal expansion mismatch, increase the interfacial strength and maintain a smooth and stable surface with the substrate. Since the adhesion layer is sandwiched between the substrate and the ZnO film, a material whose structure is close to them is also necessary. In this thesis, two elements, Ti, titanium, (a common adhesion layer with good mechanical interfacial strength) and Nb, Niobium, (lattice parameter close to ZnO), were selected as adhesion layers. Their affects on controlling the ZnO structure and properties was also investigated in this thesis.

3.2.2.2 RF Sputtering of Zinc Oxide Film

There are many sputtering parameters that can affect the microstructure of the deposited film during nucleation and growth. In this thesis, four parameters, which can be independently controlled by the PVD75 system, were studied, as tabulated in Tables 3-1. and 3-2:

(1). ZnO target radio frequency (RF) power

(2). Adhesion layer (Nb or Ti)

(3). Substrate deposition temperature

(4). Substrate bias

The materials science paradigm, processing determines structure which determines properties, was studied in this thesis.

3.2.3 Film Deposition by ALD

ALD (atomic layer deposition) was used to deposit zinc oxide films for comparative purposes. The ALD films were deposited in a Savannah 100 (Cambridge Nano Tech Inc.) ALD reactor shows in Fig. 3-2.

Figure 3-2: Photo of Savannah 100 ALD system for ZnO thin film depositions.

3.2.4 Film Deposition by PLD

Comparative zinc oxide films were also deposited by PLD (Pulsed Laser Deposition). The PLD zinc oxide films were deposited on silicon substrates by a Lambda Physik Compe201 PLD system shown in Fig.3-3. Although there are some similar parameters like power and deposition rate to sputtering, PLD can give varying ZnO stoichiometry.

Figure 3-3: Photo of Lambda Physik Compe201 pulsed laser deposition system for ZnO thin film depositions.

3.3 Film Characterization

3.3.1 Profilometer

A Veeco Dektak 150 Profilometer was used to measure the film thicknesses and the wear track depths and cross-sectional areas removed after the pin-on-disc tests. In thistechnique, a 12.3μm pin radius, 100μg force, and 800 to 1200μm scan lengths were used to measure both of these quantities.

3.3.2 X-ray diffraction (XRD) and X-ray reflectivity (XRR)

A Rigaku Ultima III diffractometer was employed for both grazing-incidence X-ray

diffraction (GIXRD) and X-ray reflectivity (XRR) studies in the parallel beam mode, which used a thin film stage and scintillation detector. Cu Kα x-rays, which have 1.54Å wavelength, were generated at 40 kV and 44 mA in the system. For all 20-90° 2θ GIXRD scans, there were some settings maintained at constant values: 5° incident angle, 0.05° step size, 2 degree/min scan speed, 10 mm divergence height limiting slit, 0.5° incident side Soller slit, open attenuator, 0.5° diffracted side parallel beam (PB) slit, and open sizes for all divergence, scattering and receiving slits (DS/SS/RS). XRR measurements were made with 0-6° 2θ and omega scans using a 10 mm divergence height limiting slit and 0.2mm for DS, SS and RS. There were no Soller and PB slits used in order to maximize signal intensity. Attenuator size was varied from 1/800 to 1/10 depending on signal intensity. Jadev7.0 and XRRv2.0 softwares were used to process the results for GIXRD and XRR respectively. The Debye-Scherrer equation, $d = 0.9\lambda / B \cos\theta$, where λ=1.54Å, B is the full-width at half-maximum height (FWHM) of the XRD peak, and θ is the Bragg angle was used to measure the grain size, d. ZnO grain sizes were studied as a function of substrate temperature, bias and interfacial film density.

3.3.3 Pin-on-Disc (POD) tribometer test

A Falex ISC200 pin-on-disc (POD) tribometer was used to measure the friction coefficient of the films and generate wear tracks under two sizes of balls (pins): 1/8 inch and 1/4 inch diameter stainless steel 440C (SS440). The former size was used on the ZnO films deposited on Si substrates, while the latter size was used on the ZnO films deposited on Ti-alloy substrates. The normal load in the POD tests was fixed at 100 grams. Table 3-3 provides the experimental POD test protocol used for the ZnO films.

SET	Normal Load (g)	Pin Ball Material	Replicates
ZnO on Silicon wafer	100	1/8” stainless steel (SS440)	≧2
ZnO on Ti alloys substructure	100	1/4” stainless steel (SS440)	≧2

Table 3-3: The pin on disc test design setting.

The POD tests were replicated at least two times on a particular film. However, the radius was changed as well as the total number of cycles to reach the same distance traveled by the steel ball. The revolutions per minute (RPM) is also adjusted when the radius of the test is changed, in order to maintain the linear speed constant at 2.1 cm/s for all POD tests.

3.3.4 Optical Microscopy

A Nikon Eclipse ME600 optical microscope was used for imaging the surfaces of steel balls and the wear tracks from 10X to 50X magnifications immediately after POD testing. The NIS-Elements BR2.30 software is needed to process the images and measure the width of the wear track.

3.3.5 Scanning Electron Microscopy

A FEI-Nova scanning electron microscope (SEM) was used to image the ZnO surfaces, wear tracks and debris after POD testing. SEM was also used to see if plastic deformation occurred inside the ZnO wear tracks. The focused ion beam (FIB) inside the SEM was used to generate cross-sectional samples inside and outside the wear tracks to study the ZnO solid lubrication mechanisms.

3.3.6 Transmission Electron Microscopy

An FEI Co. Tecnai G2 F20 S-Twin 200keV field-emission scanning transmission electron microscope (S/TEM) was used to characterize the structure, ZnO lattice d-spacing, and ZnO grain orientation inside and outside the wear track.

CHAPTER 4

RESULTS AND DISCUSSION

This chapter presents experimental results and discussion of the zinc oxide (ZnO) thin film deposition and characterization analyses. In addition, the tribological behavior of the ZnO films on Si and Ti alloys is presented along with the tribological mechanisms responsible for solid lubrication. Based on the results, ZnO has the potential to be used as a solid lubricant in load bearing applications such as orthopedic implants.

4.1 Thin Film Condition Selection

The ZnO films were first deposited on Si wafers to study the role of structure in controlling the tribological properties (coefficient of friction and wear factor). Approximately 500nm thickness ZnO films were deposited on an adhesion layer of Nb or Ti (~80nm thickness) under varying sputtering conditions, as outlined previously in Tables 3-1 and 3-2. The coefficient of friction (COF) results on various ZnO thin films were first considered to identify what deposition conditions resulted in lower friction and also.[30]

4.1.1 ZnO Thin Film on Si Wafer under Various Radio Frequency Power with No Bias at Room Temperature

This set of experiments varied the radio frequency (RF) power to sputter deposit ZnO thin films on silicon wafers, in order to determine how RF power affects ZnO structure and tribological properties. These films were deposited under 5mTorr pure Ar gas with various RF powers from 50 to 200 watts without direct current (DC) bias on the substrate at room temperature. Figure 4-1 presents the (a) grazing-incidence X-ray diffraction (GIXRD) spectra, (b) deposition rate, and grain size of the zinc oxide films as a function of RF sputter power.

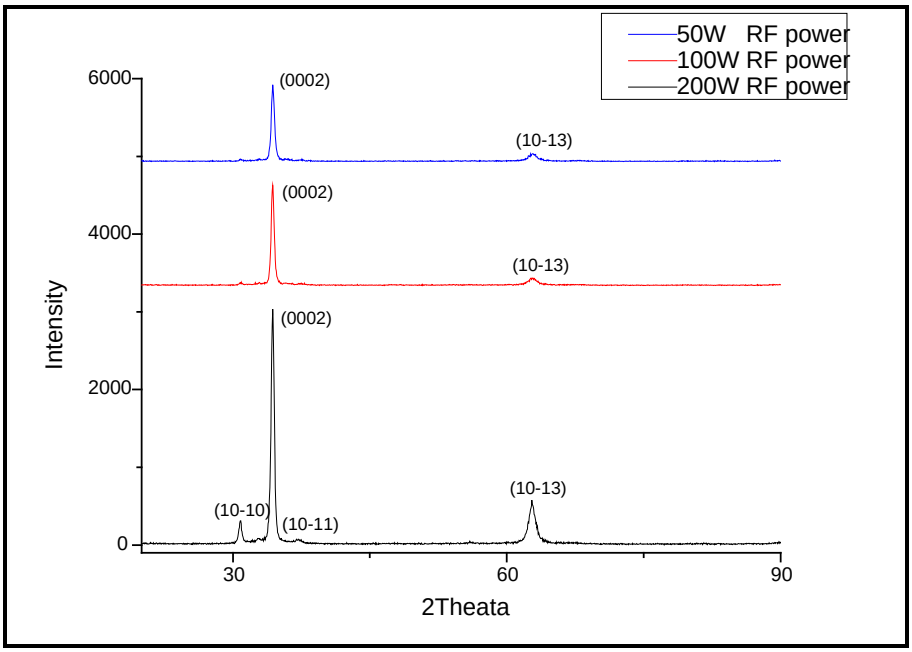

(a)

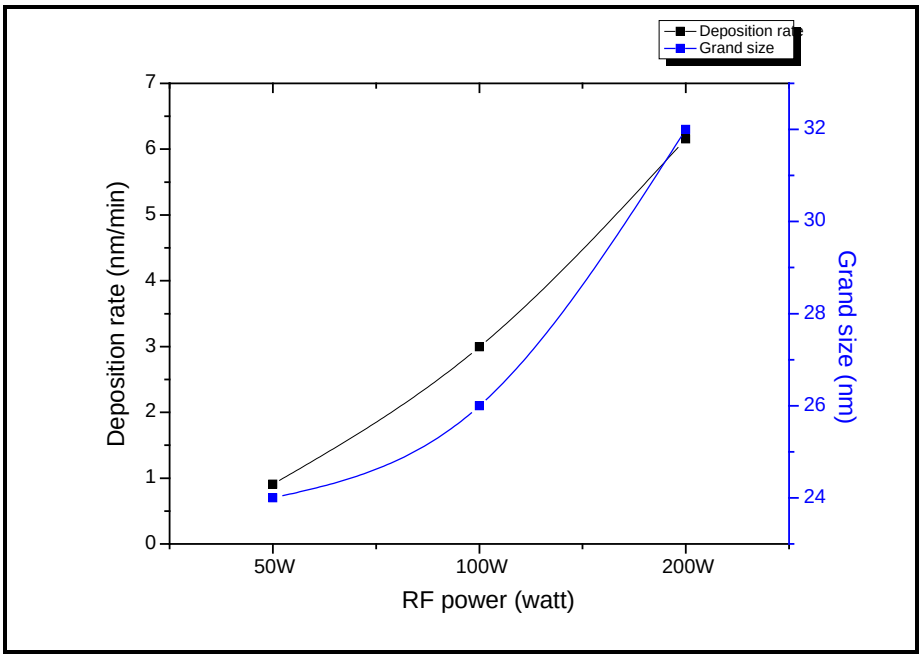

(b)

Figure 4-1: GIXRD spectra of ZnO films as a function of RF power (a), deposition rate and grain size of ZnO films (b). The figures show that the intensity of (0002) peak, deposition rate, and grain sizes of the films all increasing RF power.

From the GIXRD data, there is a very strong preferred orientation of ZnO crystallites (texture) active at 2Θ ~ 34.3 degrees that belong to (0002) orientated grains, and the intensity of the (0002) reflections is enhanced with increasing RF power. In addition, the deposition rate and grain size of the ZnO films also increase with increasing RF power. These trends are corroborated from a study by Filckynegerova[31]. They mentioned that the deposition rate of the films is linear with increasing RF power because the number of atoms bombarded from the target corresponds to the RF power. In addition, it was reported that the peak intensity increased with power since it improved the crystallinity of the films, which is supported by the increasing grain size. However, there was a threshold power according to Filckynegerova, in which the increasing trend of ZnO film intensity was achieved the highest RF power of 400 watts. Increasing the power further reduced the intensity of the (0002) peak, while other weak diffraction intensity peaks like (10-10) and (10-11) were now present. The reason for this phenomenon is the higher RF power will force a reduction of the preferred orientation of ZnO crystallites and the texture is lost and thus the crystallites become more randomly orientated, In this thesis, the RF power was not increased above 200 W since the (0002)-orientated crystallites wanted to be preserved due to their good tribological behavior. The (0002) texture, also named c-axis orientation because the basal plane is perpendicular to the substrate normal of growing ZnO films. This texture is very common in ZnO films made by different methods because the basal plane is the most densely packed and thermodynamically preferred in the wurtzite structure[32]. To determine which of the three sputtering RF powers resulted in the best tribological performance, pin-on-disc (POD) testing was done to screen the films. Figure 4-2 shows optical microscope images of ZnO films after tribometer testing based on the POD conditions in table 3-3. The image in (a), which has the lowest RF target power of 50W, shows that there is a large amount of deformation and loose debris inside and outside the wear

track and on the steel ball, which caused the high steady-state coefficient of friction (μ_{ss}) of ~0.8, as well as third body abrasive wear. Similarly for the 100 W film POD surfaces shown in image (b) with the same μ_{ss}, there is extensive wear of the ball and inside the wear track accompanied by copious amounts of debris. Thus, both of these films deposited with either 50W or 100W RF target power are not good candidates for further sputtering runs and analysis. In contrast, the 200W RF power deposited ZnO film exhibited half μ_{ss}~0.4 and consequently the amount of wear on the ball and inside the wear track was minimized as evident by the images shown in Figure 4-2c. Also, there was no obvious sign of any debris inside the wear track. Therefore, the high RF power of 200W resulted in the best tribological properties. This high RF power, previously shown in Figure 4-1a, exhibited the highest intensity of (0002) texture, since the 200W power resulted in higher ion impact energy during sputtering thus increasing the density of the film. This also shows the importance of the (0002) texture in achieving low friction and wear.

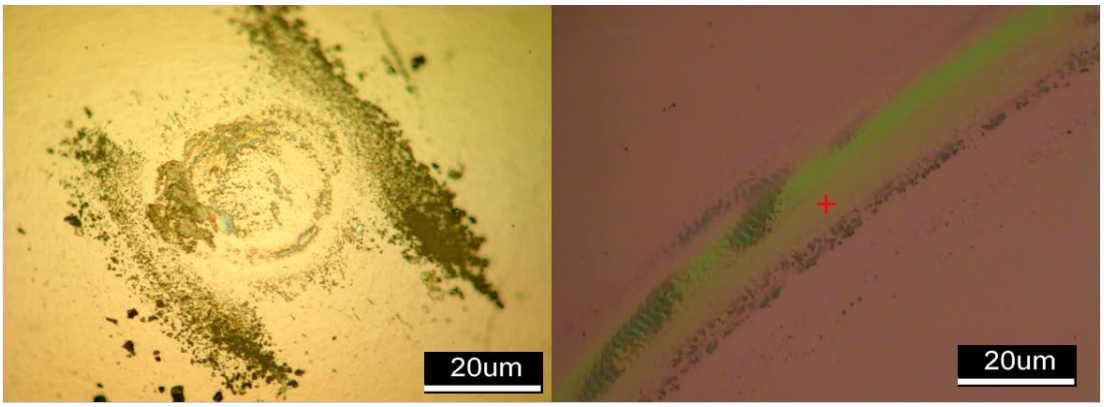

(a)

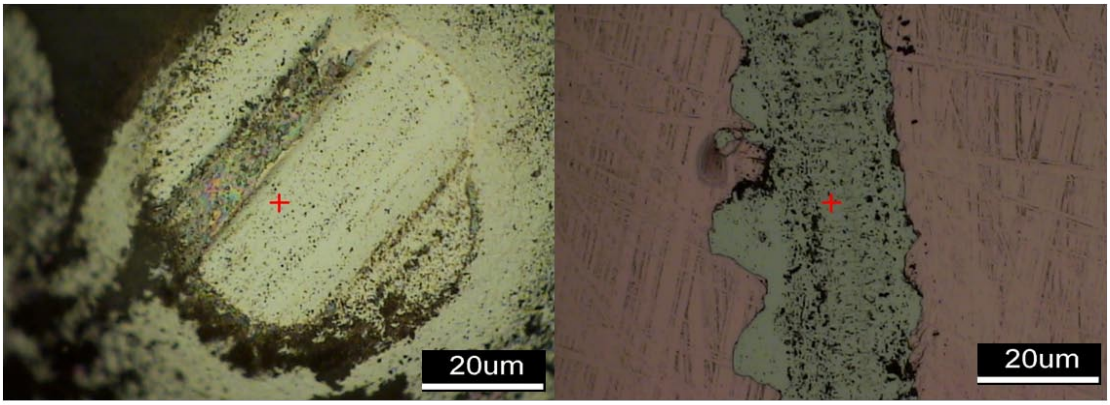

(b)

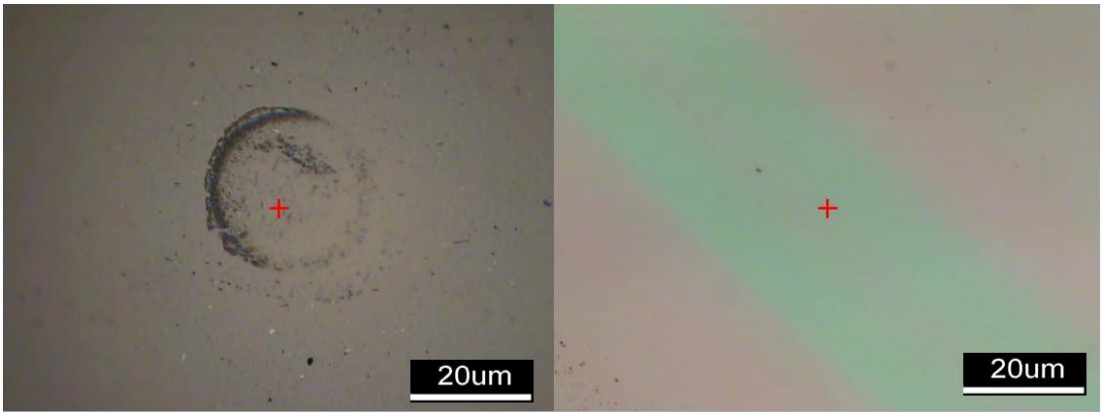

(c)

Figure 4-2: Optical microscope photos of zinc oxide thin films after POD tribometer testing. RF sputtering power: (a) 50W, (b) 100W, and (c) 200W.

4.1.2 ZnO Thin Film on Si Wafer under 200W Radio Frequency Power with Various Conditions

Since the higher RF sputtering power of 200W resulted in the best tribological properties, it will be used as the power for the remainder of the ZnO depositions in this thesis to further study the role of substrate temperature, bias, and adhesion layer material on ZnO structure and tribological properties. While this approach may seem incremental, it is necessary in order to determine the best film deposition parameters for optimal tribological properties. Tables 4-1 and 4-2 summarize the GIXRD reflection peaks observed for the ZnO films that were made under 200W power with either Nb adhesion layer or Ti adhesion layer, respectively, under varying substrate temperature and bias previously listed in chapter three. If only one GIXRD peak is listed in the tables, then the film has preferred orientation with this reflection. The tables also list the corresponding μ_{ss} values.

Condition		GIXRD Peaks	μ_{ss}
Room Temp.	No Bias	(0002)	0.4
Room Temp.	Bias -25V	(0002)	0.45
Room Temp.	Bias -50V	(0002) ,(10-10),(10-11), (10-12),(11-20),(20-20)	0.4
Room Temp.	Bias -75V	(10-10),(11-20),(20-20)	0.6
Room Temp.	Bias -100V	(10-10),(10-11),(20-20)	0.55
400C	No Bias	(0002)	0.45
400C	Bias -50V	(0002)	0.38
400C	Bias -100V	(10-10), and (10-11)	0.5

Table 4-1: The GIXRD reflection peaks and corresponding μ_{ss} values of the ZnO films with Nb adhesion layer under varying deposition conditions.

Condition		GIXRD Peaks	μ_{ss}
Room Temp.	No Bias	(0002)	0.5
Room Temp.	Bias -25V	(0002)	0.68
Room Temp.	Bias -50V	(10-10),(10-11), (11-20),(20-20)	0.7
Room Temp.	Bias -75V	(11-20)	0.7
Room Temp.	Bias -100V	(10-10)	0.8
400C	No Bias	(0002)	0.45
400C	Bias -100V	(10-10),(10-11), (11-20)	0.56

Table 4-2: The GIXRD reflection peaks and corresponding μ_{ss} values of the ZnO films with Ti adhesion layer under varying deposition conditions.

Several trends are noted based on the results shown in the two tables. First, the ZnO films deposited with 200W RF power, Nb adhesion layer, and -50V bias at 400C exhibited the lowest friction followed closely by the film deposited at room temperature under same conditions. Second, the role of substrate temperature (room temperature versus 400C) does not significantly influence the grain orientation or μ_{ss} values. Third, substrate bias voltage is the major sputtering experimental parameter that affects the ZnO grain orientation which in turn affects the μ_{ss} values. Fourth, the μ_{ss} values are lower when the ZnO films exhibit (0002) texture. ZnO films with (0002) texture have lower friction because (0002) nano-columnar grains have low surface energy, low interfacial shear strength, and thus have low friction[33,34]. Substrate bias sputtering can enhance the density of films and thus may be able to extend the wear life of the films. X-ray reflectivity (XRR) was used to determine if an increase in ZnO density was obtainable with biasing. From the analysis, the density of the ZnO film with -50V bias sputtering was determined to be 5.45±0.60 gm/cc,

based on the spectrum shown in Figure 4-3a, while the film without bias sputtering was lower at 5.14±0.41 gm/cc, spectrum shown in Figure 4-3b. Compared to the theoretical bulk ZnO density of 5.61 gm/cc, bias sputtering does help increase the density closer to this theoretical value.

(a)

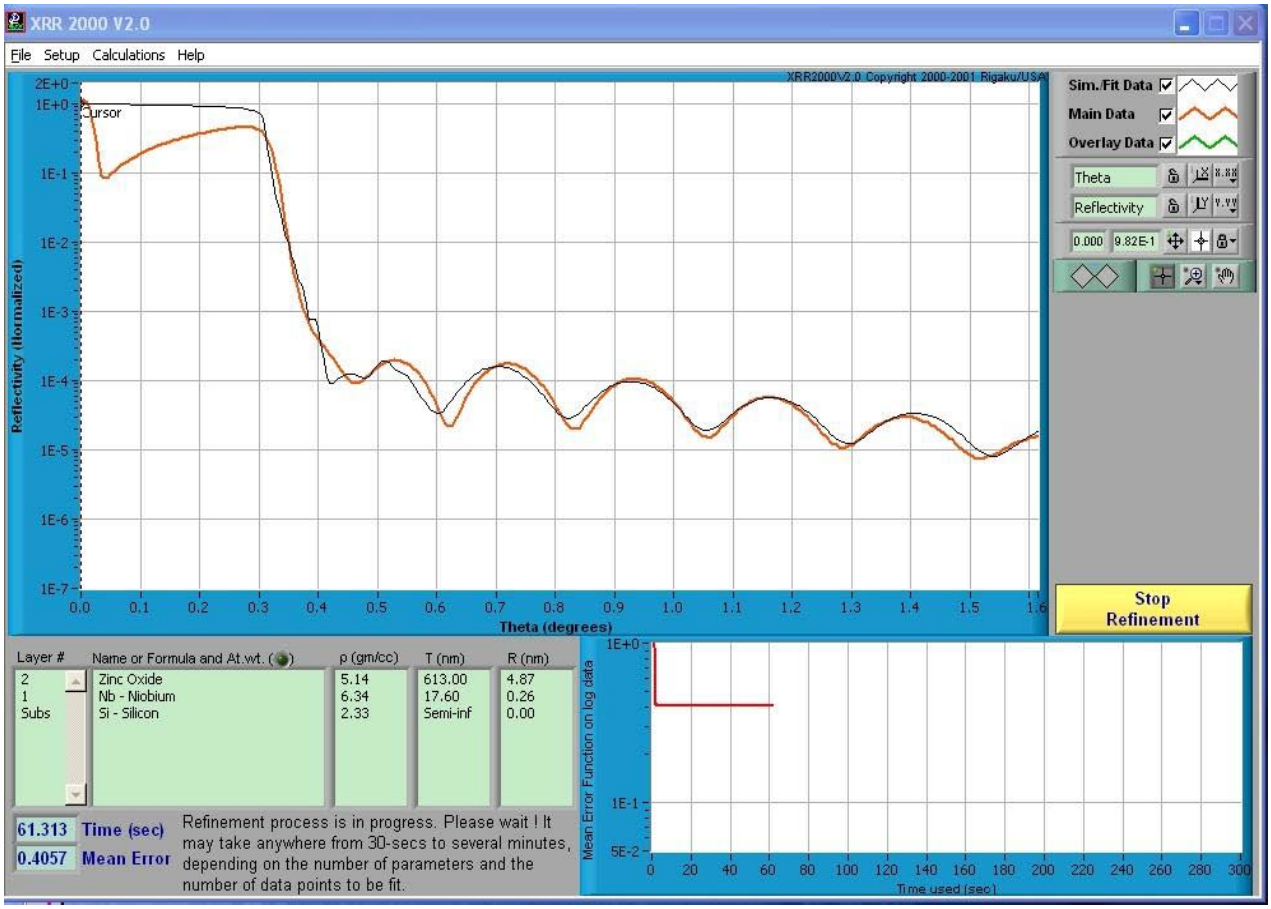

(b)

Figure 4-3: The XRR spectra of the ZnO film deposited (a) with -50V substrate bias, and (b) without bias.

However, bias sputtering not only affects the film density but also the ZnO structure (different grain orientations). The intensity of (0002) textured grains starts to decrease while other multiple orientations, such as (10-10), (10-11), (10-12), (11-20), and (20-20) appear, or grow in intensity, when the substrate bias voltage is increased. Figure 4-4 shows the GIXRD spectra of ZnO films as a function of varying substrate bias. There is a loss of (0002) texture to randomly orientated grains when the substrate bias is greater than -50V.

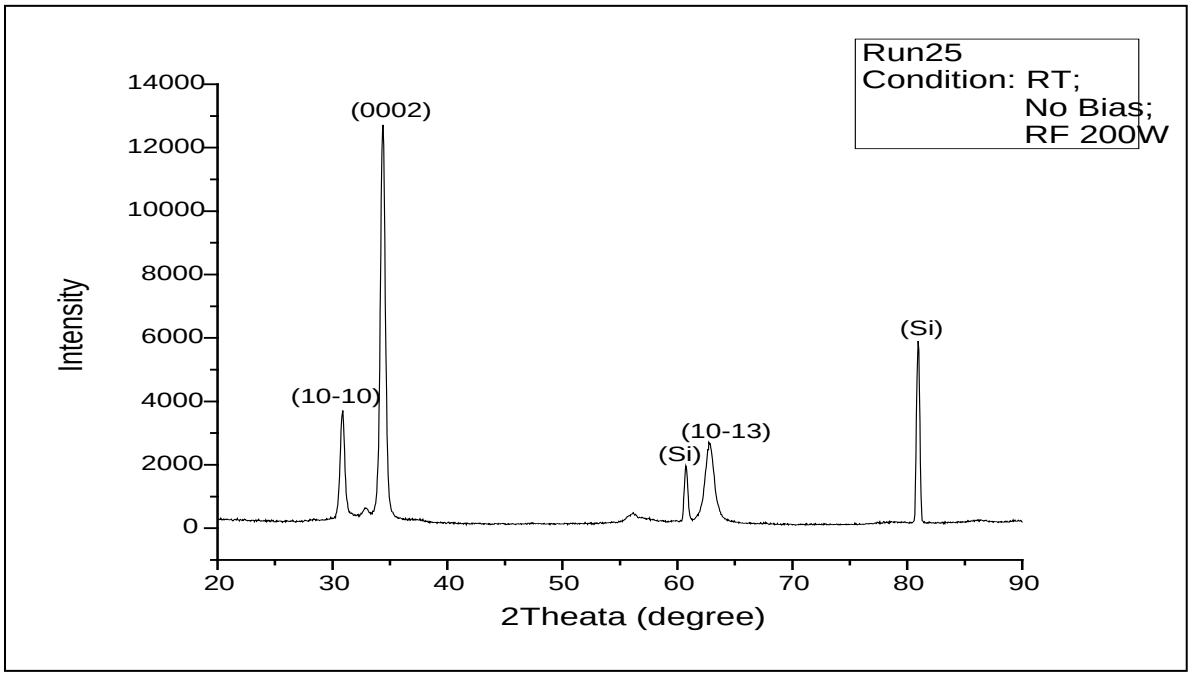
Run25
Condition: RT;
No Bias;
RF 200W
Intensity
2Theata (degree)
(0002)
(10-10)
(Si)
(10-13)
(Si)
14000
12000
10000
8000
6000
4000
2000
0
20
30
40
50
60
70
80
90

(a)

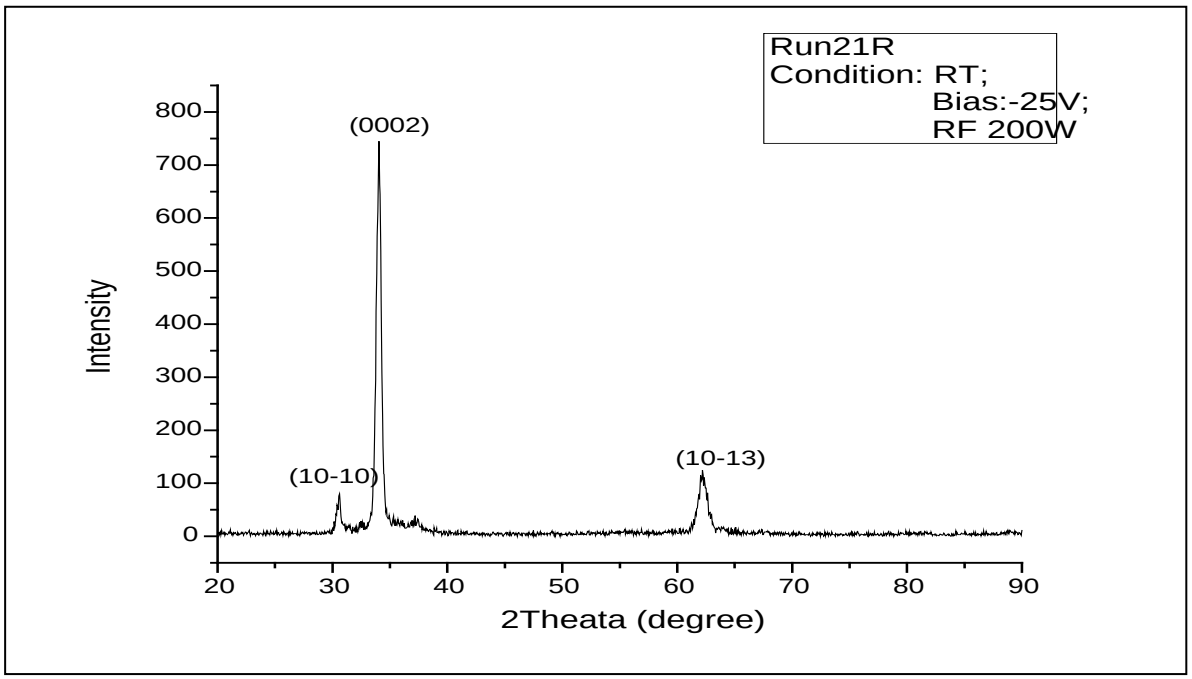
Run21R
Condition: RT;
Bias:-25V;
RF 200W
Intensity
2Theata (degree)
(0002)
(10-10)
(10-13)
800
700
600
500
400
300
200
100
0
20
30
40
50
60
70
80
90

(b)

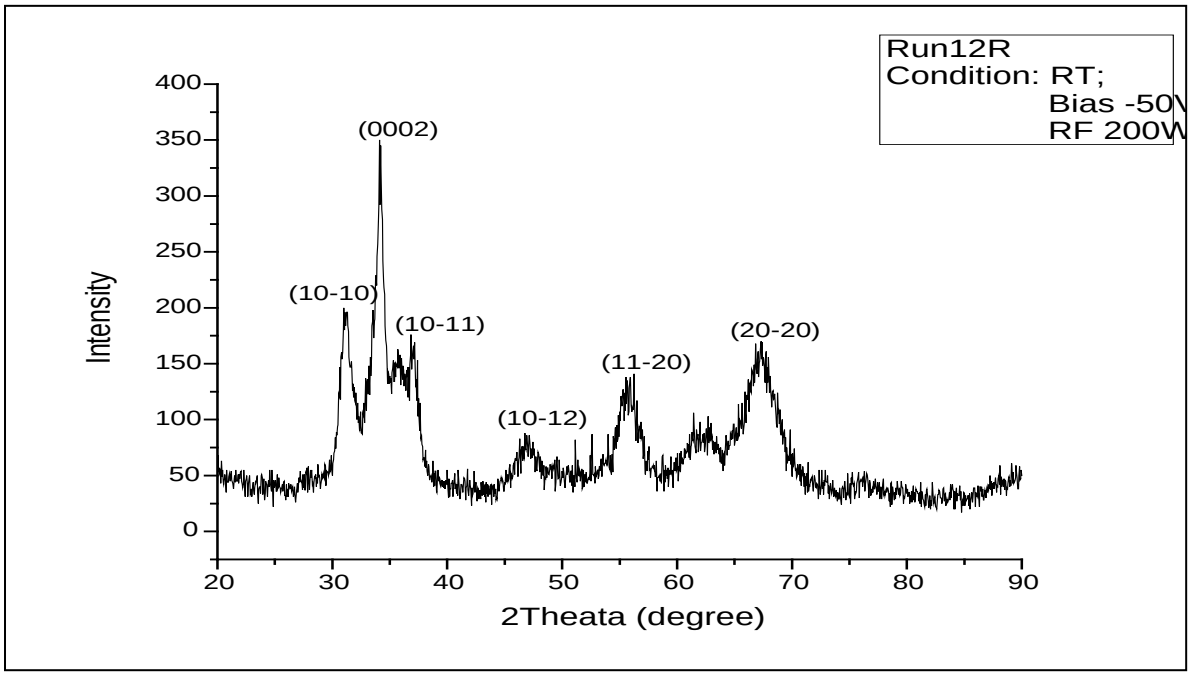
Run12R
Condition: RT;
Bias -50V
RF 200W
Intensity
2Theata (degree)
(0002)
(10-10)
(10-11)
(10-12)
(11-20)
(20-20)
0
50
100
150
200
250
300
350
400
20
30
40
50
60
70
80
90

(c)

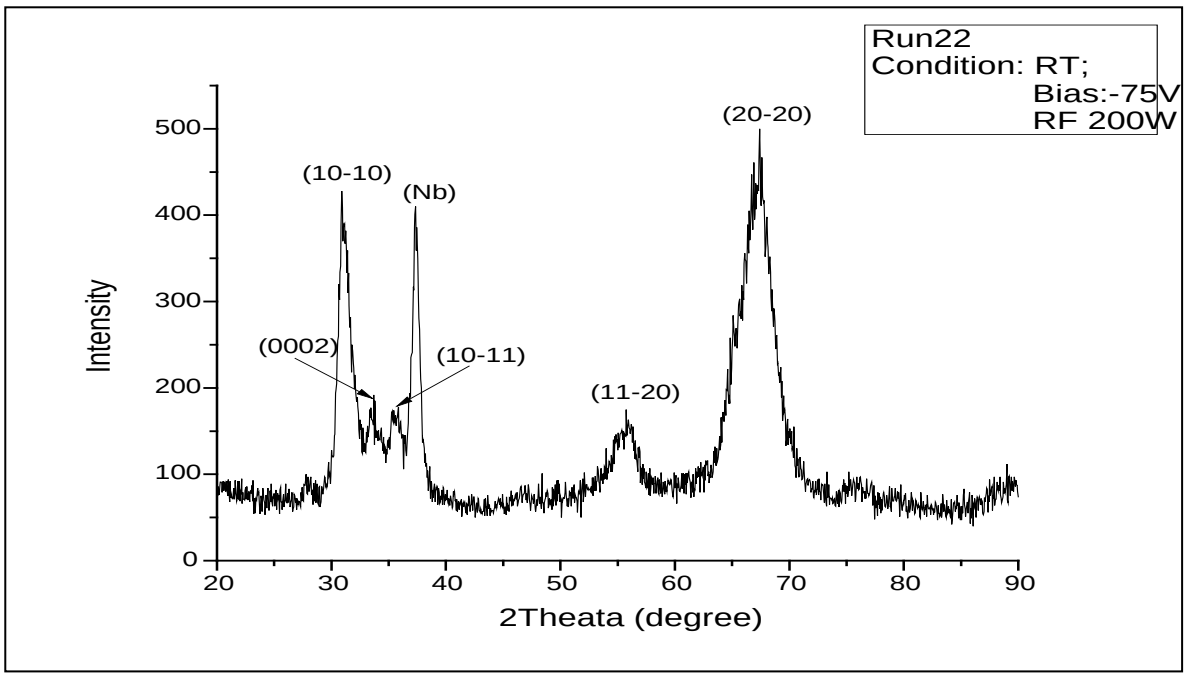
Run22
Condition: RT;
Bias:-75V
RF 200W
Intensity
2Theata (degree)
(0002)
(10-10)
(Nb)
(10-11)
(11-20)
(20-20)
0
100
200
300
400
500
20
30
40
50
60
70
80
90

(d)

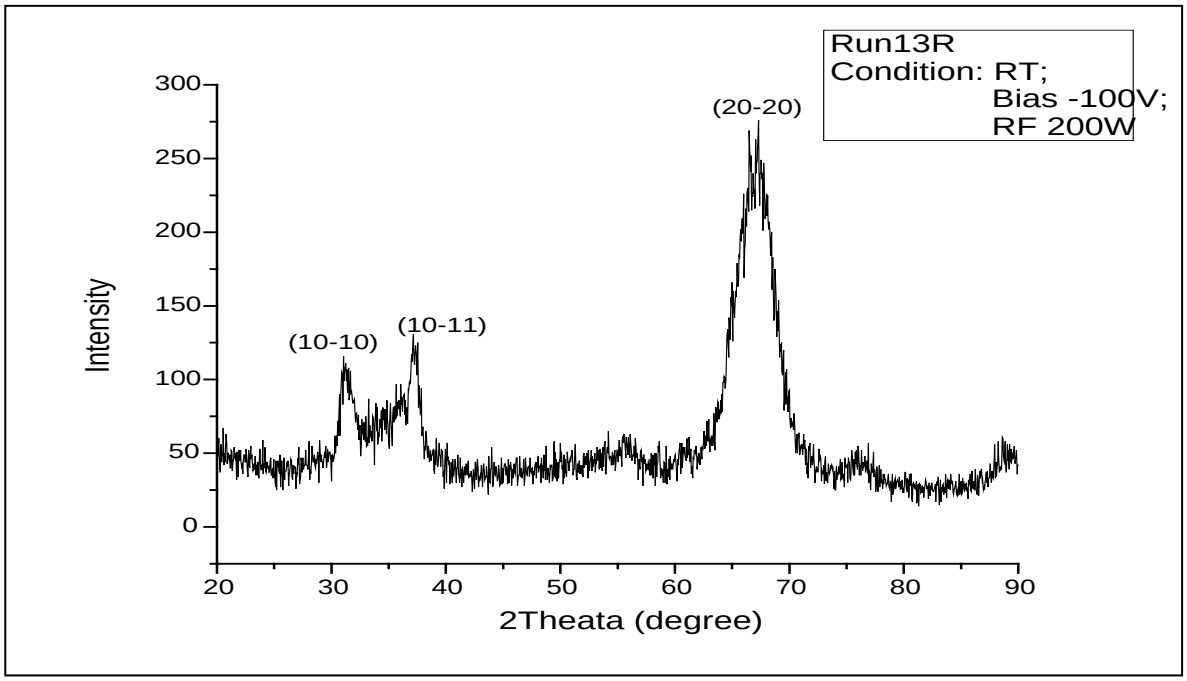

(e)

Figure 4-4: XRD spectra of ZnO films as a function of bias voltage: (a) bias 0V, (b) bias -25V, (c) bias -50V, (d) bias -75V, and (e) bias -100V.

With continued bias voltage to -75 and -100 V, other randomly orientated grains replace the (0002)-orientated grains and for the -100 V film the (0002) reflection is lost. Therefore, the threshold substrate bias voltage is - 50 V to preserve ZnO (0002) texture. POD tests as a function of substrate bias voltage determined that the -50V bias film exhibited the lowest μ_{ss} value of 0.4 followed by the -25 V bias film at μ_{ss}~0.45. The -75 V and -100 V films had higher μ_{ss} values of 0.6 and 0.55, respectively. This behavior substantiates the effect that (0002)-orientation nano-columnar grains reduce friction. Wear factor is another tribological property to measure the wear behavior of the films, in which a low wear factor represents good wear resistance. The wear factor = wear volume loss inside the wear tracks (mm^3) / normal load (N) * wear distance (m).[30] Figure 4-5 shows that the ZnO film wear factor on Nb adhesion layer agrees with the

aforementioned friction behavior where the -50V bias film has the best wear resistance. Figure 4-5 also compares the wear factor of the ZnO films as a function of adhesion layer (Nb and Ti). The wear resistance of the ZnO films on the Nb adhesion layer is superior to the respective films grown on the Ti adhesion layer. The ZnO film on Nb adhesion layer has better wear resistance since there is a loss of (0002)-orientated grains with biasing using Ti adhesion layer due to lattice parameter mismatch during film growth. Thus, there appears to be a tradeoff between (0002)-orientated grains and substrate bias voltage. A threshold of -50V bias with some (0002)-orientated grains on Nb adhesion layer results in the best tribological performance. Figure 4-6 shows a comparison of ZnO wear factors with Nb adhesion layer as a function of various deposition conditions. The film deposited at 400C with - 50V bias has the lowest wear factor followed closely by the film deposited under the same conditions at room temperature, which agrees with the previously mentioned coefficient of friction behavior. Based on these results, this sputtering condition for ZnO films was selected for deposition on Ti-alloys.

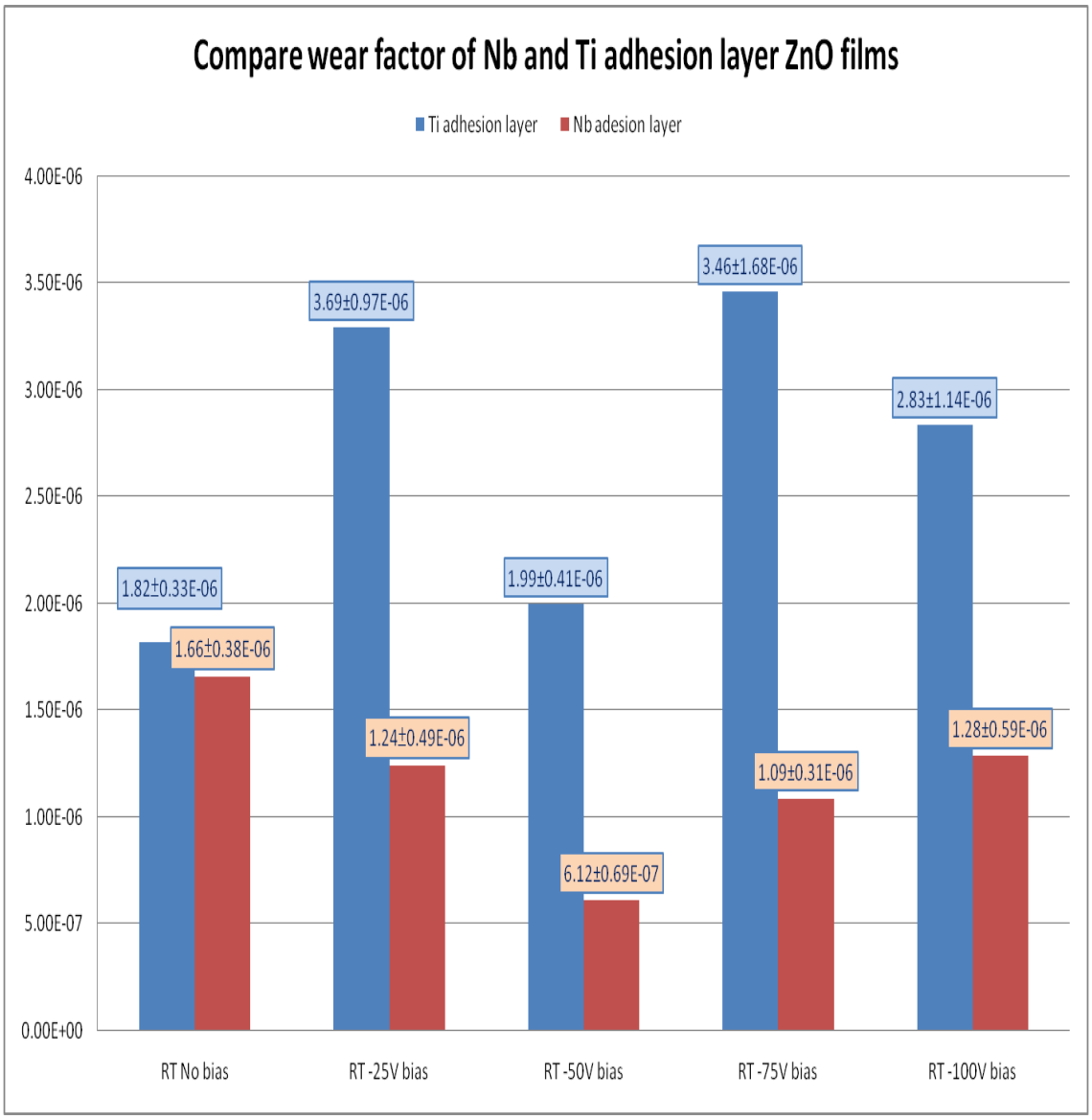

Figure 4-5: Comparison between wear factors of ZnO films on Nb and Ti adhesion layers.

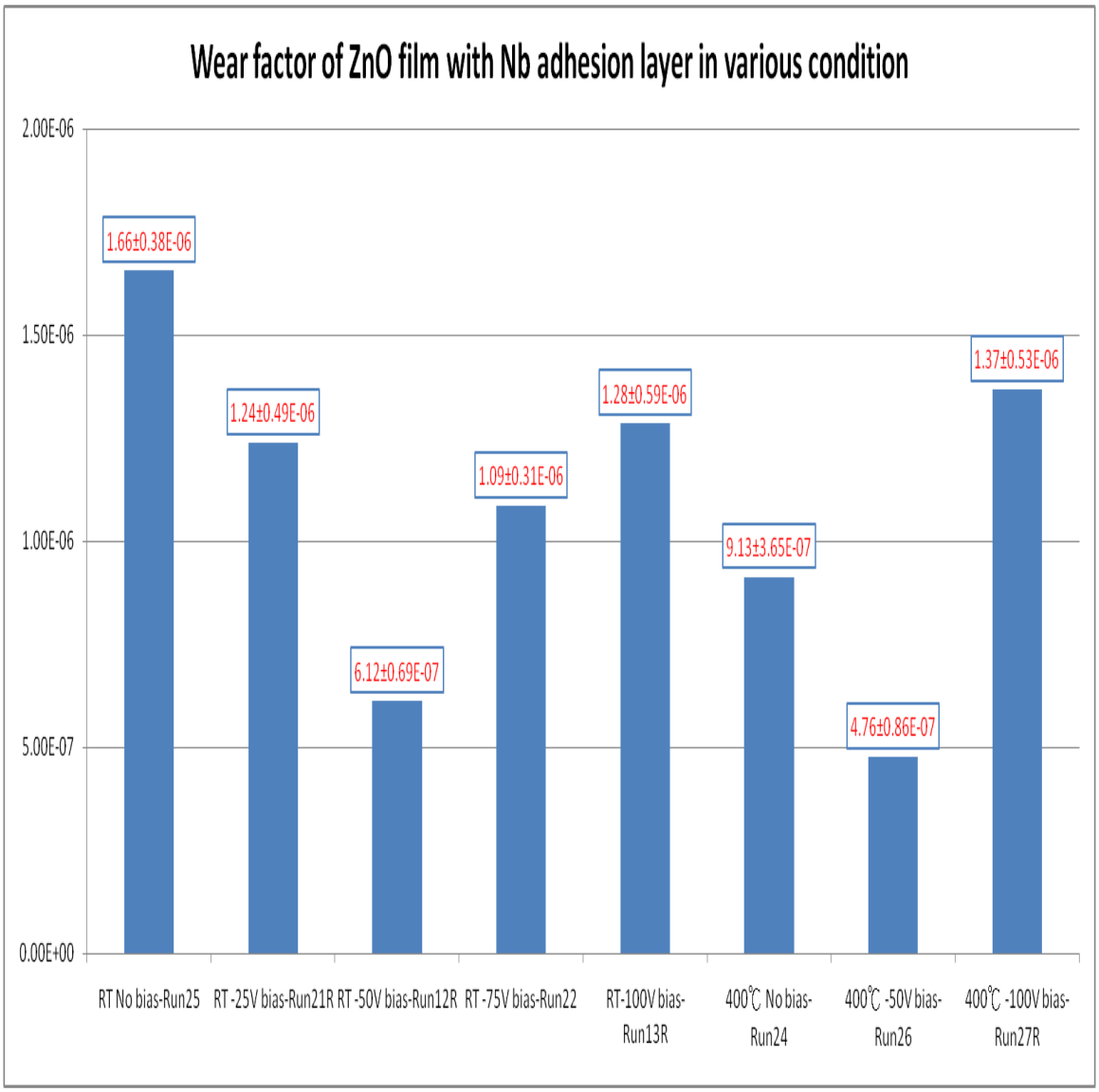

Figure 4-6: Comparison of wear factors of ZnO films on Nb adhesion layer as a function of various deposition conditions. The film deposited at 400C with - 50V bias has the lowest wear factor.

4.2 ZnO Coatings Deposited on Ti-Alloys

In this section, sputtered ZnO films were grown on three Ti-alloy substrates TNZT+2B, Ti-6Al-4V, and (CP)-Ti. The ZnO films were deposited on Nb adhesion layers at a RF power of 200 W with a substrate temperature of 400C and -50 V bias. The structure, tribological behavior,

solid lubrication mechanisms, and different deposition methods of ZnO films will be presented and discussed in this section.

4.2.1 The Structure of ZnO Films on Ti Alloys

The X-ray diffraction (XRD) spectra of ZnO films sputtered on Ti alloys, titanium-niobium-zirconium-tantalum + TiB precipitate (TNZT+2B), Ti-6Al-4V and commercially pure (CP)-Ti are presented in Figures 4-7, 4-8, and 4-9, respectively. For all the Ti-alloys, there are ZnO (0002)-orientated grains, but no texture (preferred orientation) exists. Instead of (0002) texture in the ZnO films, the XRD spectra show ZnO has multiple randomly orientated grains, most noticeably the (10-10), (0002), and (10-11). Other phases from the Ti-alloy substrates, such as TiB, α-Ti and β-Ti, are also shown in the XRD spectra.

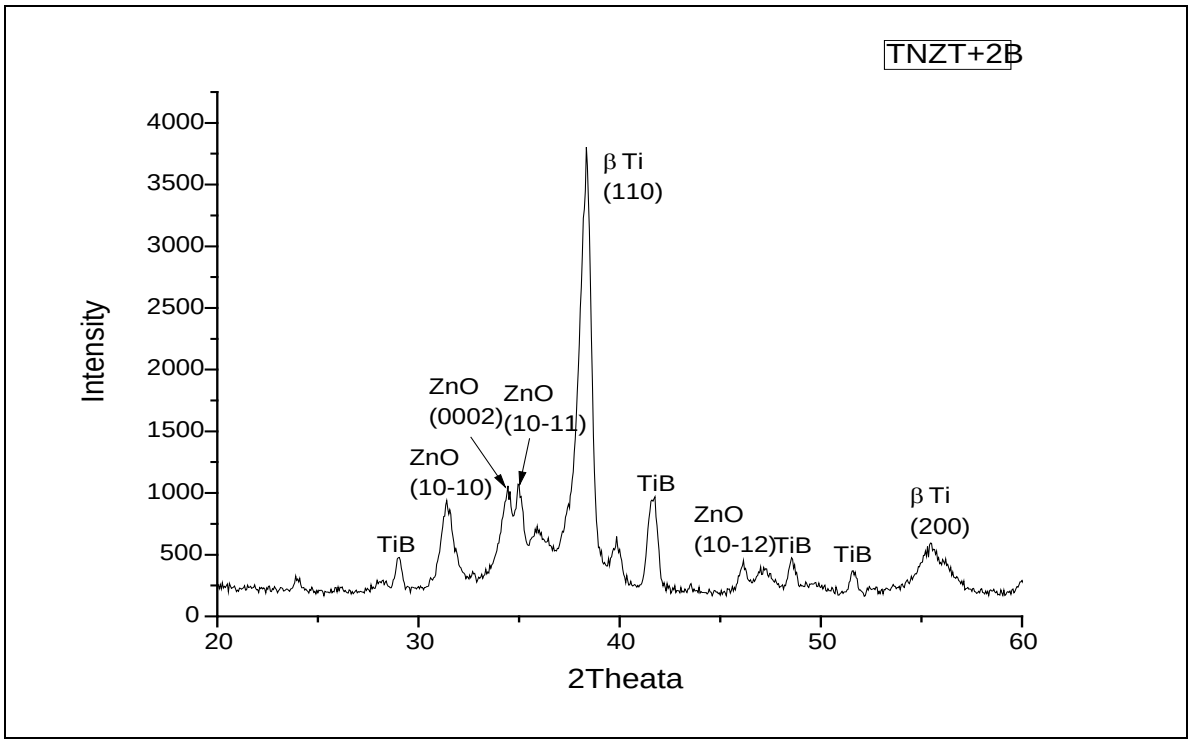

Figure 4-7: XRD spectrum of ZnO film sputtered on Ti alloy, TNZT+2B.

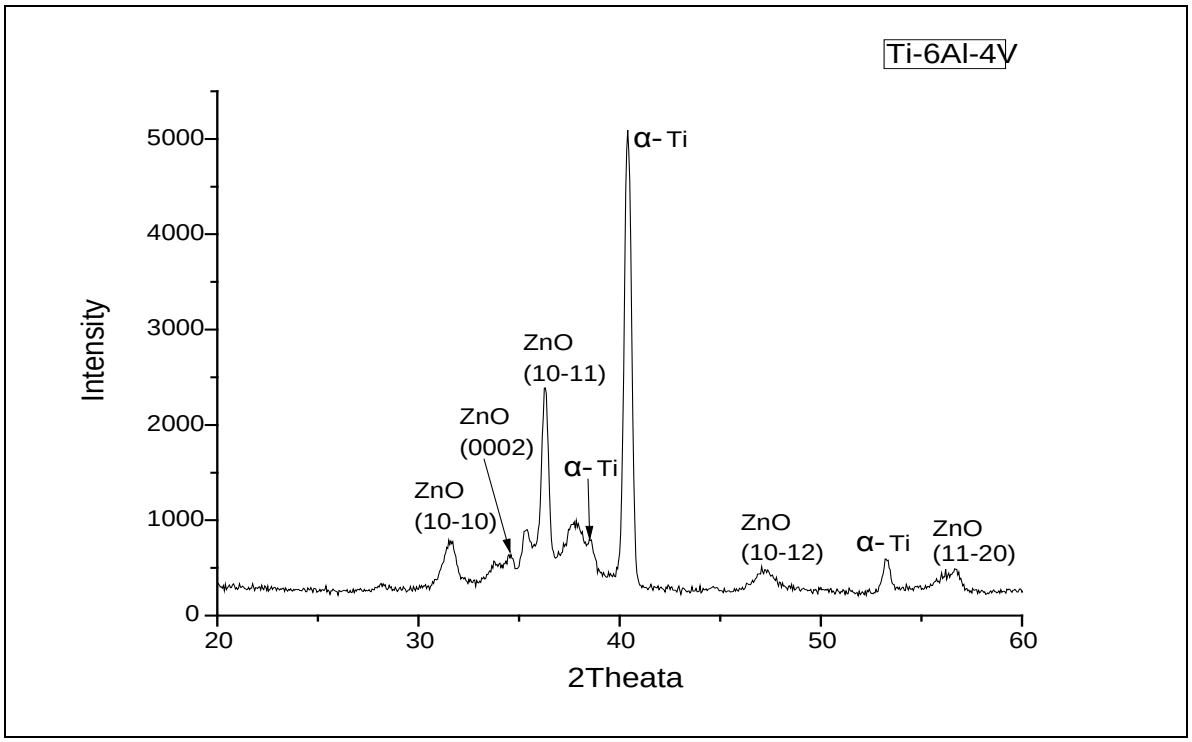

Figure 4-8: XRD spectrum of ZnO film sputtered on Ti alloy, Ti-6Al-4V.

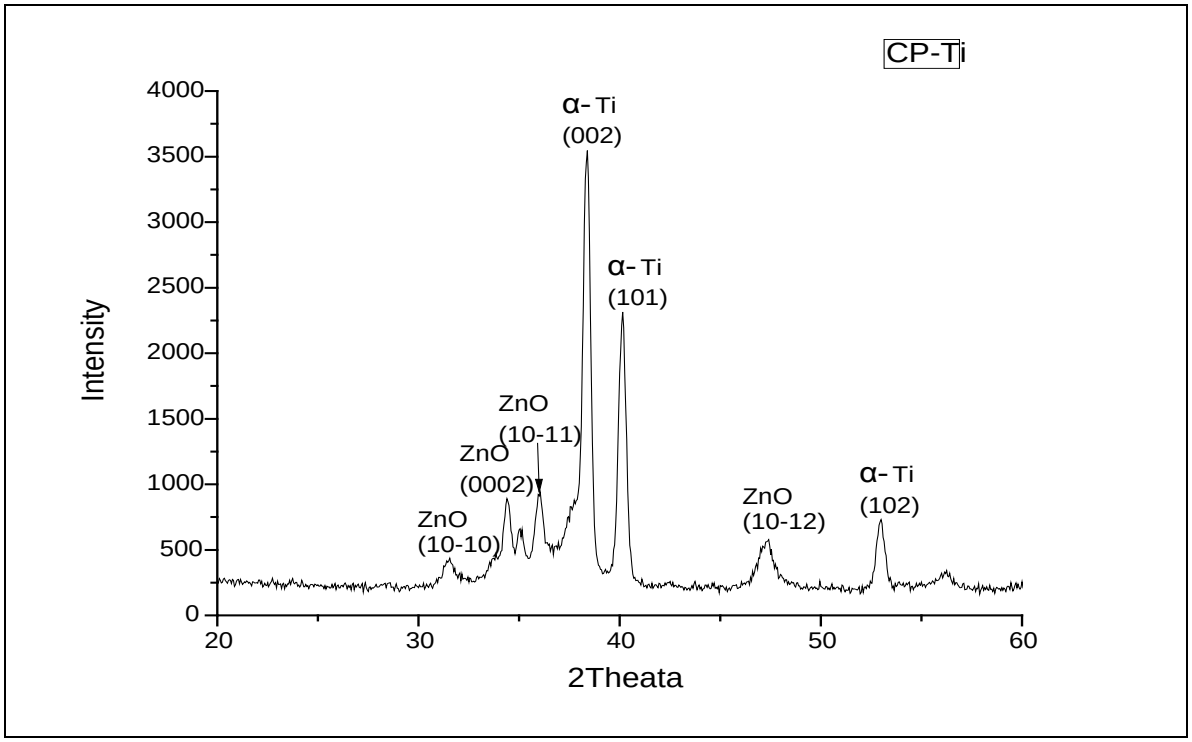

Figure 4-9: XRD spectrum of ZnO film sputtered on Ti alloy, CP-Ti.

4.2.2 Wear Behavior of ZnO Coated and Uncoated Ti Alloys

The ZnO films on Ti alloys substrates were tested in the POD tribometer according to the experimental setup in Table 3-3. The testing allows for a comparison between wear tracks and wear factors of bare Ti alloys and ZnO coated Ti alloys to confirm if ZnO films can improve the wear resistance of bare Ti alloys. Figure 4-10 are optical microscope images of the wear tracks of bare Ti alloys and ZnO coated Ti alloys taken at the end of the POD tests. It is evident that smaller wear track widths and less wear debris exist when the Ti alloys are coated with ZnO in comparison to the uncoated Ti alloys. This confirms that the ZnO films contributed to the enhanced wear resistance of bare Ti alloys. In addition, the wear factors of each test were calculated and are shown in Figure 4-11. The wear factors of ZnO films are three to four orders of magnitude smaller than the wear factors of bare Ti alloys. A wear factor on the order of 10^{-3} is considered severe wear, while 10^{-5} is considered mild wear and 10^{-6} to 10^{-7} is considered low wear. Based on these regimes, the ZnO coated Ti-alloys all exhibit low wear compared to their respective uncoated Ti alloy. Of the Ti alloys, TNZT+2B exhibited the lowest wear factor uncoated and ZnO coated due to the TiB hard precipitates on the surface and subsurface improving the abrasive wear resistance. These results confirm that the sputtered nanocrystalline ZnO films provide excellent wear protection of the bare Ti alloys.

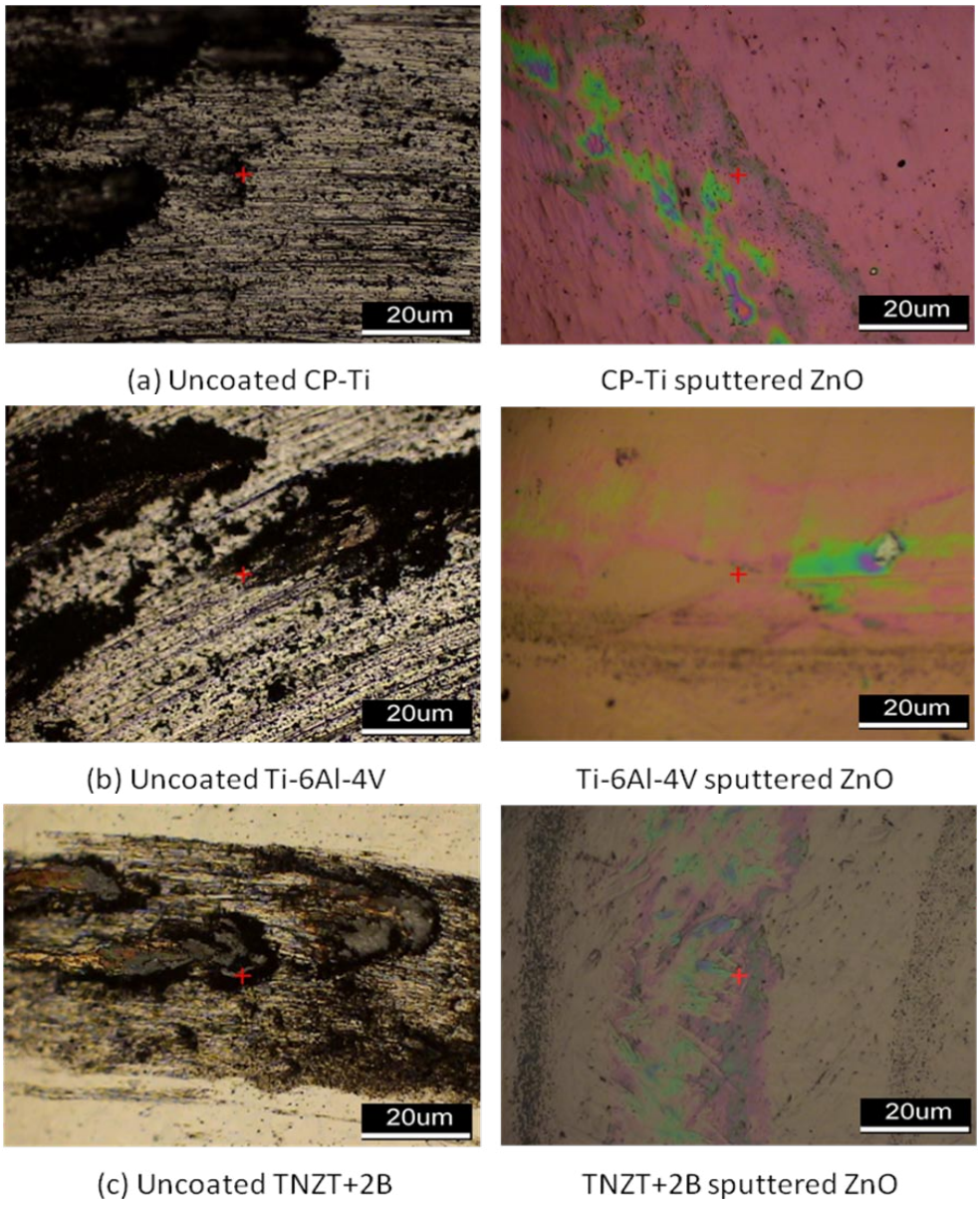

Figure 4-10: Optical microscope wear track images of uncoated Ti alloys and sputtered ZnO coated Ti alloys, (a) uncoated CP-Ti and sputtered ZnO on CP-Ti, (b) uncoated Ti-6Al-4V and sputtered ZnO on Ti-6Al-4V, (c) uncoated TNZT+2B and sputtered ZnO on TNZT+2B.

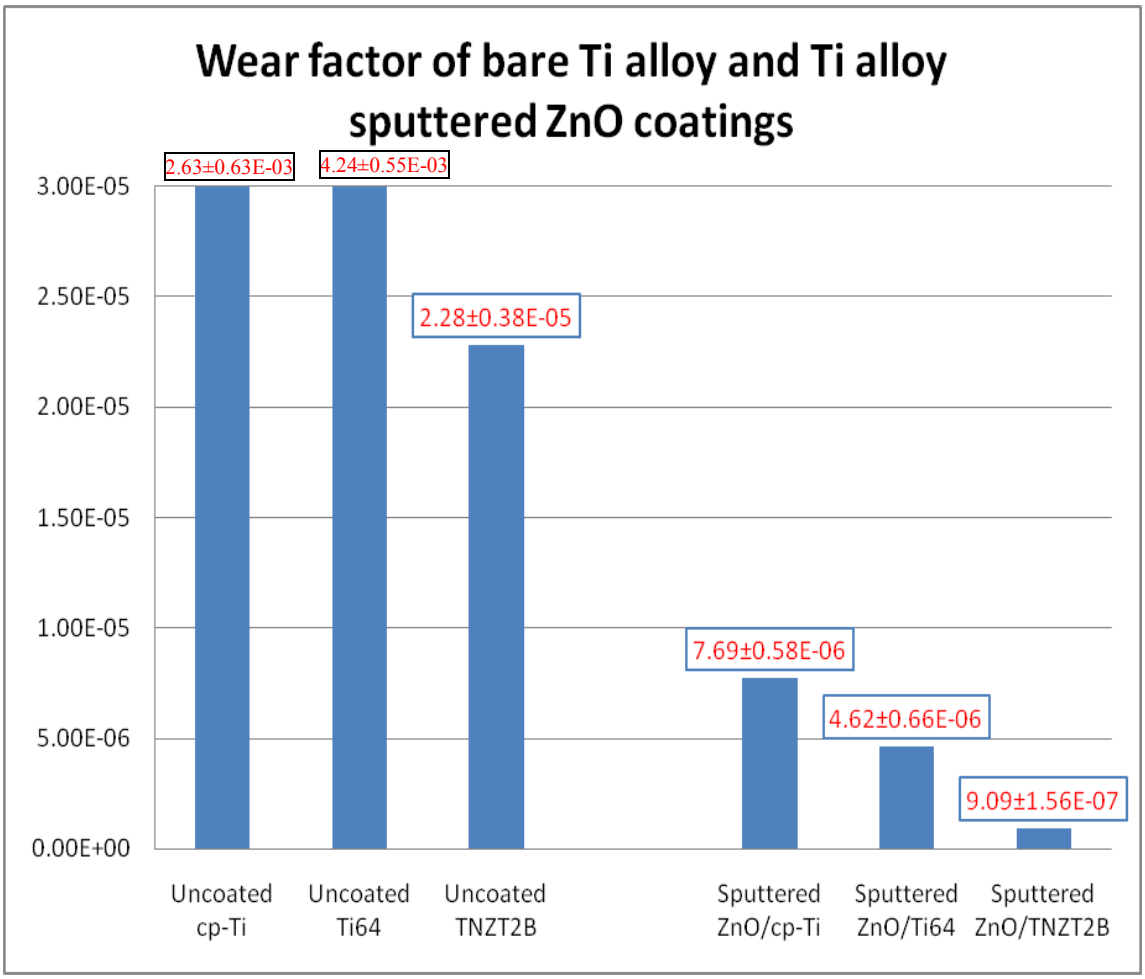

Figure 4-11: Wear factors of ZnO coated and uncoated Ti-alloys.

4.2.3 Wear Behavior Comparison of Different Deposition Techniques

ZnO wear factors were compared to determine which deposition technique resulted in the lowest friction and wear. The ZnO deposition techniques compared to sputtering are pulsed laser deposition (PLD), another physical vapor deposition (PVD) technique, and atomic layer deposition (ALD), a chemical vapor deposition (CVD) technique. It is difficult for a perfect comparison between the techniques since each has its own subtleties; however, it was determined that the chemical composition of the ZnO films for each deposition method was 1:1 and the structure was composed of nano-columnar grains with some (0002)-orientated grains. Figure 4-12

shows the wear factors of ZnO films deposited by sputtering, ALD, and PLD. The wear factor of ZnO film sputtered has the lowest value at $9x10^{-7}$ mm^3/Nm followed closely by ALD at $1.5x10^{-6}$ mm^3/Nm and slightly higher wear factor at $7.7x10^{-6}$ mm^3/Nm. All of these wear factors fall in the low wear regime. Further analysis between the different techniques is beyond the scope of this thesis.

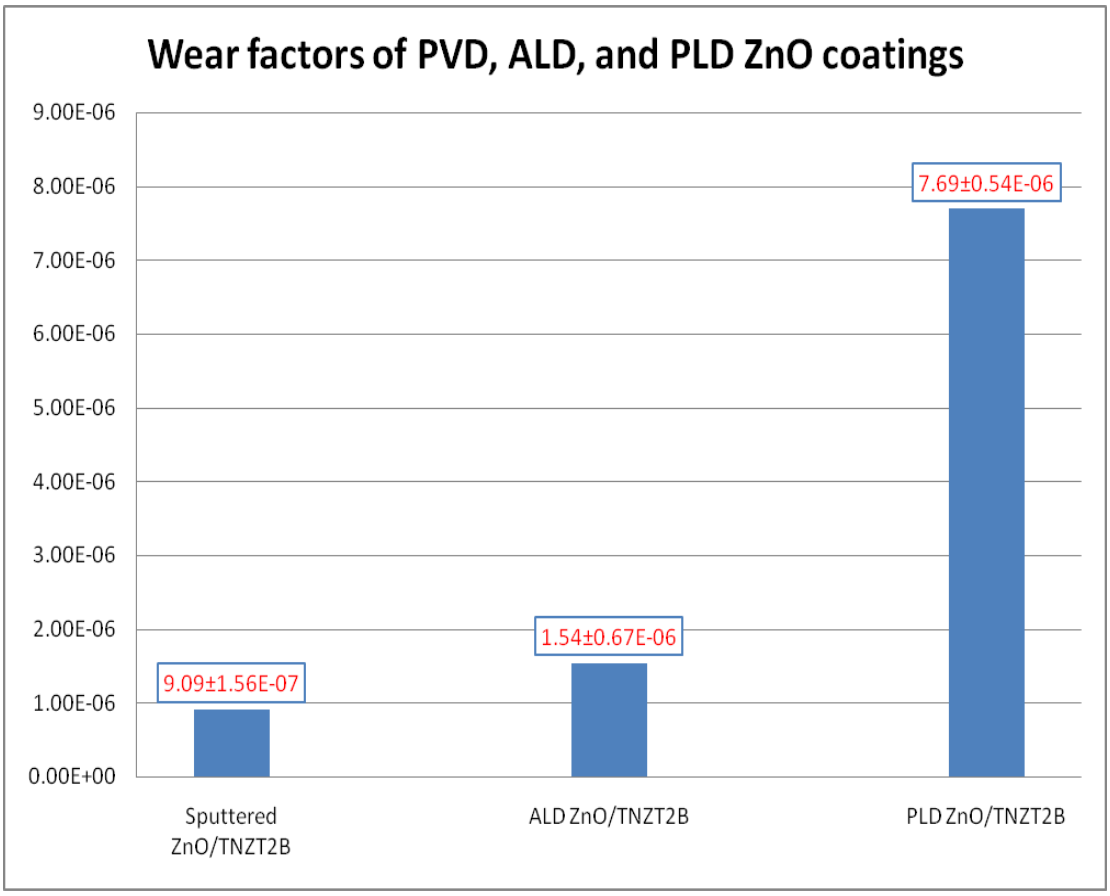

Figure 4-12: ZnO wear factors comparing different deposition techniques sputtering (PVD technique), atomic layer deposition (CVD technique), and pulsed laser deposition (PVD technique).

The following is an analysis of the solid lubrication mechanisms responsible for lubricity in nanocrystalline oxides. Figure 4-13 shows a high resolution scanning electron microscopy

(HRSEM) image of the ZnO wear track on TNZT+2B, which also shows the location of the cross-sectional focused ion beam (FIB) cut. The inset image shows a low magnification cross-sectional transmission electron microscopy (XTEM) image of the FIB-cut. The protective Pt layer is deposited inside the SEM to protect the sputtered ZnO surface during Ga^+ ion beam cross-sectional milling. Below the Pt layer is a ~450 nm ZnO layer deposited on Nb adhesion layer (not clearly seen at this magnification but shown below in TEM). The interfaces between the sputtered layers and TNZT+2B substrates are relatively sharp at this magnification.

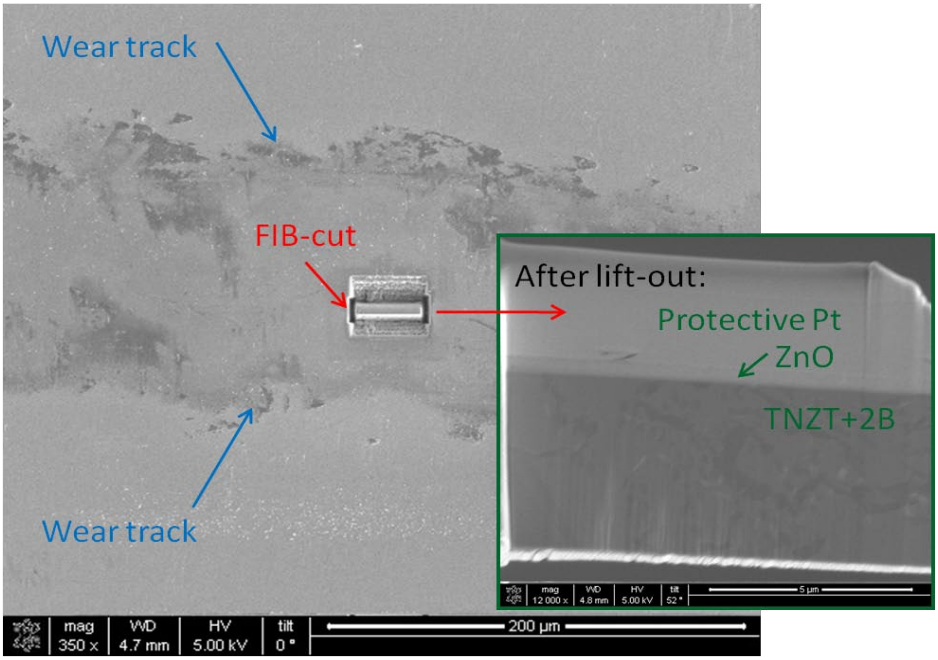

Figure 4-13: HRSEM image of ZnO wear track on TNZT+2B showing location of cross-sectional FIB-cut. Inset image shows a low magnification XTEM image of the FIB-cut displaying the sputtered layers.

Figure 4-14(a) shows the cross-sectional TEM (XTEM) image of unworn/outside wear track ZnO film and Figure 4-15(a) shows the XTEM image of worn/inside wear track film (image taken from location in Figure 4-13) after sliding to 10,000 cycles. Based on comparing the unworn versus worn images, several observations can be made on the apparent effects of cyclic sliding:

a). There is smoothing of the worn surface;

b). There is minimal thinning and hence very low wear inside the wear track;

c). A very thin wear-induced surface layer (white color) was formed with non-uniform thickness;

d). Increased amount of plastic deformation {likely dislocations denoted by orange arrows in Figure 4-15(a)};

e). No evidence of cracking or brittle fracture;

(a) Before POD test (unworn):

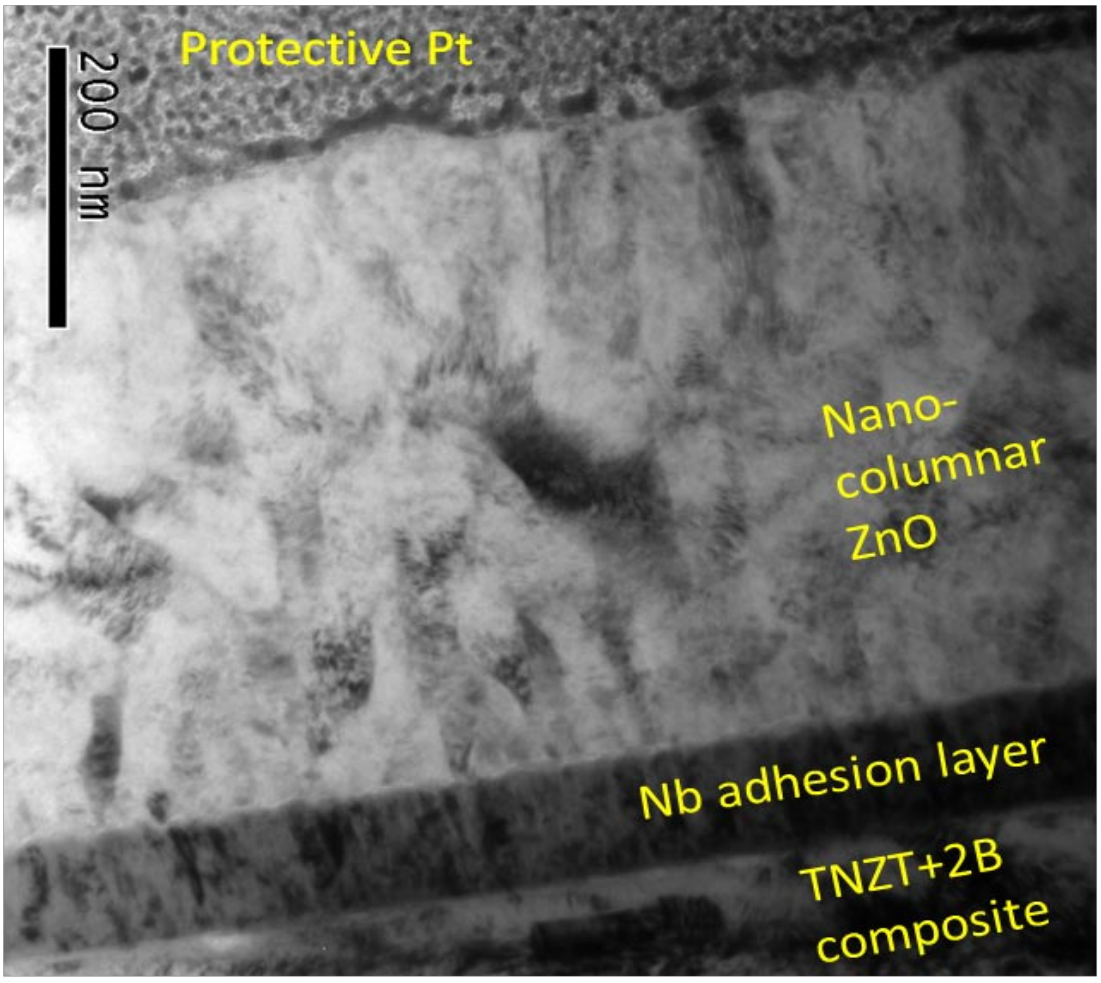

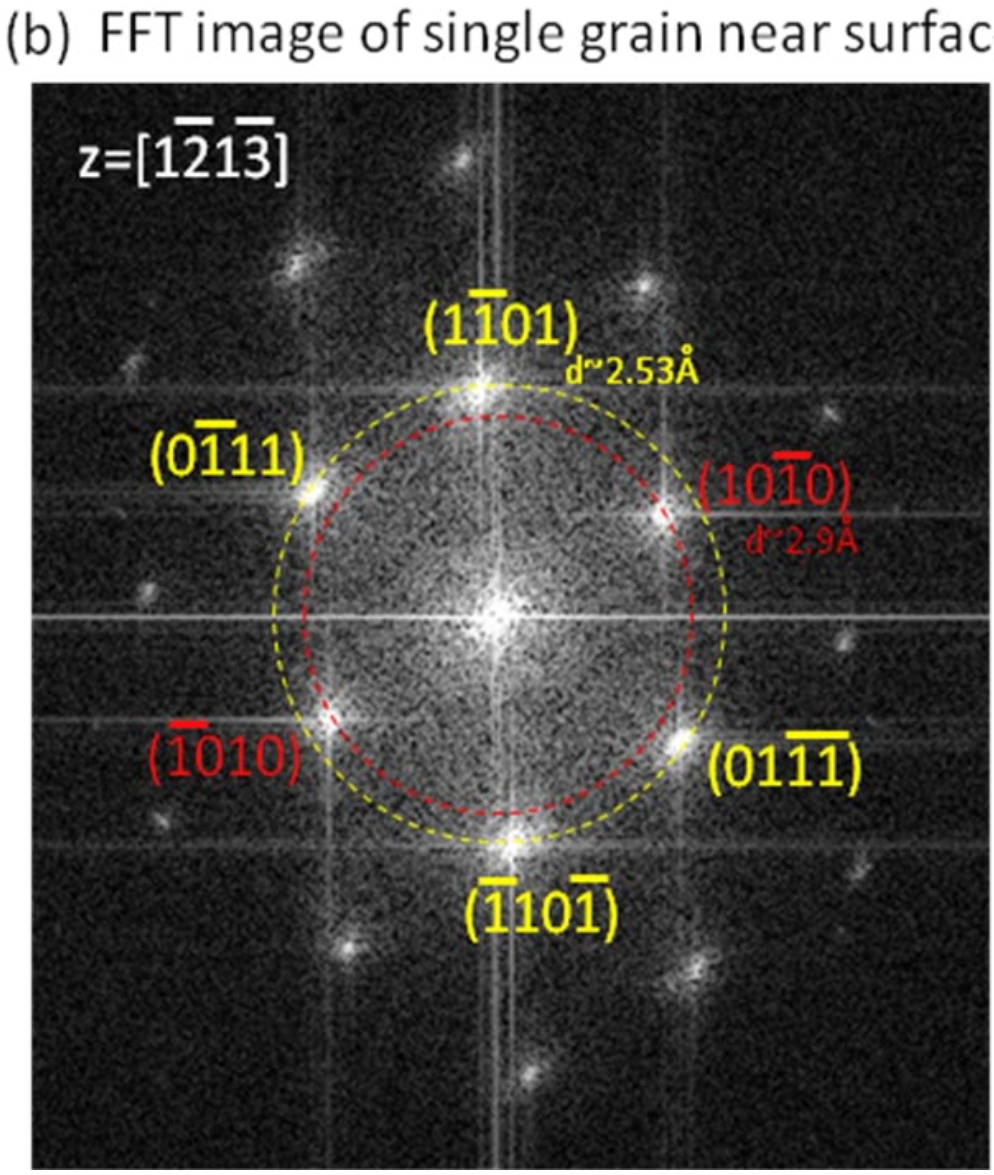

Figure 4-14: (a) XTEM image of ZnO outside the wear track (unworn). The interfaces of the sputtered layers and TNZT+2B substrate are clearly shown. Image shows nano-columnar grains (smaller near bottom) with no texture near surface. (b) Corresponding indexed electron diffraction pattern (FFT image) of single ZnO nano-columnar grain near the surface looking down the zone axis, z=[1-21-3]

(a) After POD test (worn):

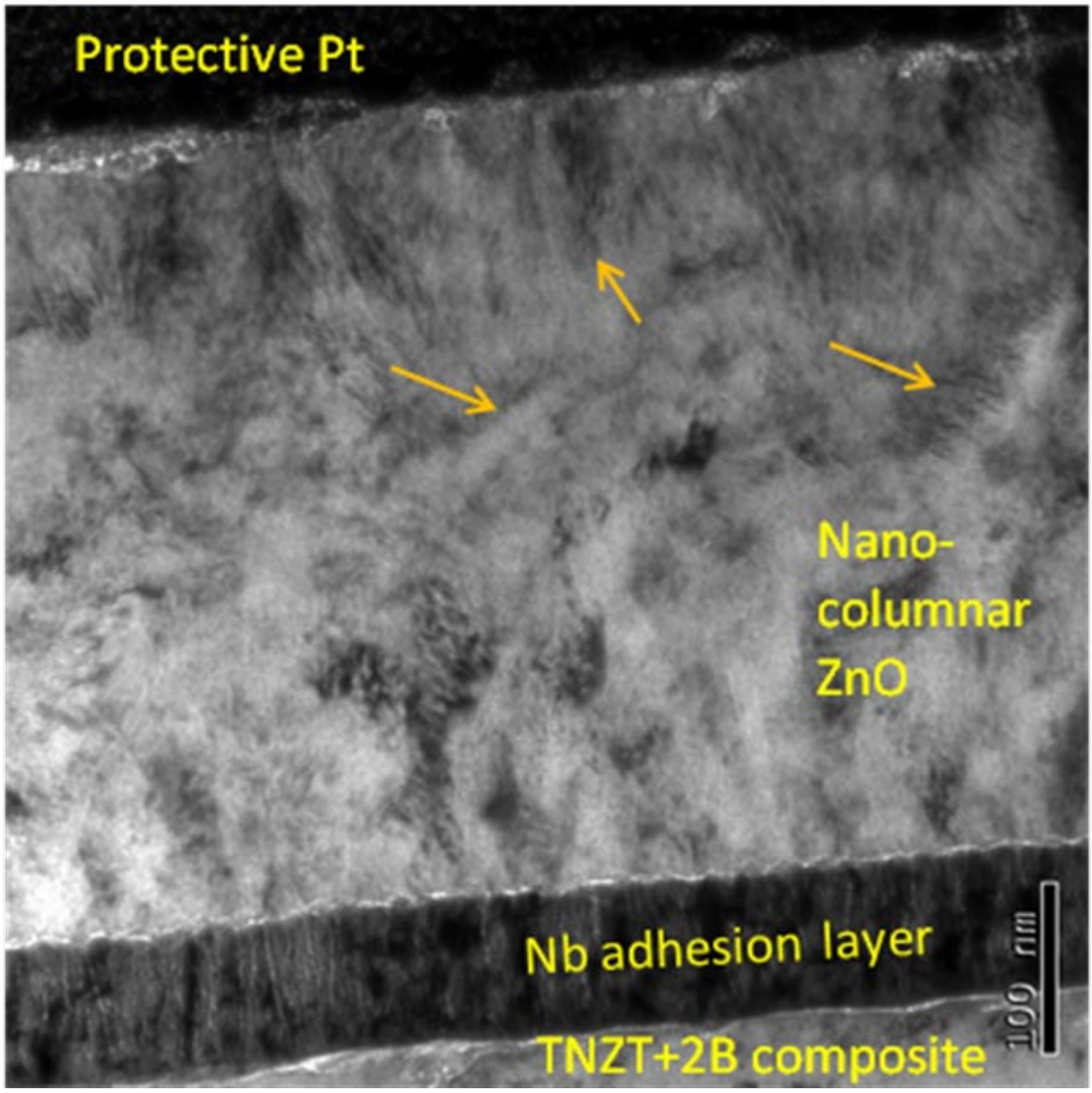

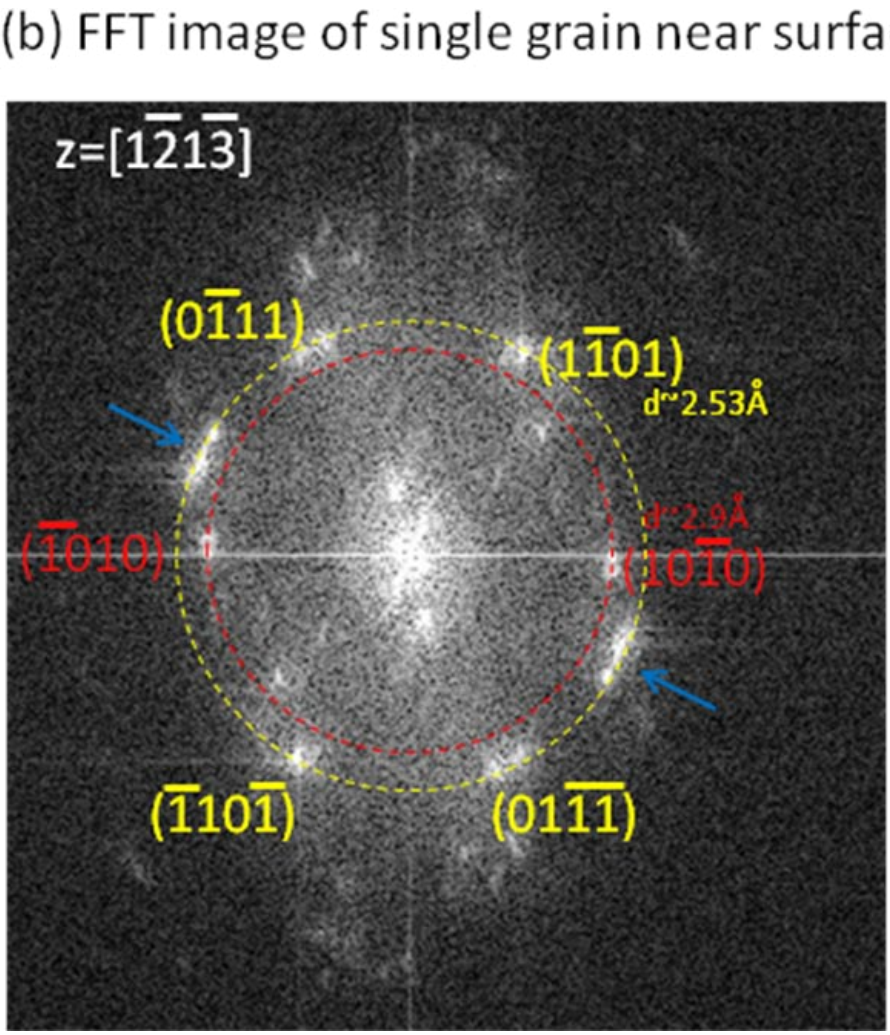

Figure 4-15: (a) XTEM image of FIB-cut shown in Figure 4-13 for ZnO inside the wear track (worn). The interfaces of the sputtered layers and TNZT+2B substrate are clearly shown. Image shows that the grains underwent considerable deformation (denoted by orange arrows) in addition to the smoothing of the surface. (b) Corresponding electron diffraction pattern (FFT image) of single columnar grain near the surface. (b) Corresponding indexed electron diffraction pattern (FFT image) of single ZnO nano-columnar grain near the surface looking down the zone axis, z=[1-21-3]. Blue arrows show additional diffraction spots indicative of multiple, finer scale grains with

local rotation due to the tribological stress/strain-induced sliding process.

Another way that the ZnO film deforms under load is not visible in the XTEM images thus far presented. This is illustrated through a comparison of the electron diffraction patterns (fast fourier transforms (FFT) images) taken of the unworn and worn films. Figure 4-14(b) shows the electron diffraction pattern (FFT image) of a single columnar grain near the surface in the as-deposited (unworn) ZnO film. The concentric rings around the diffracted spots indicate that the grain is indeed a single crystal. The zone axis, z, is the electron beam direction. Indexing the pattern determined that the d-spacings of $\{10\bar{1}0\}$ planes are ~2.90Å and $\{10\bar{1}1\}$ planes are ~2.53Å, which are in good agreement with powder diffraction file (PDF#01-075-1533) for zincite, ZnO. Figure 4-15(b) shows the electron diffraction pattern (FFT image) of a single columnar grain near the surface inside the wear track (worn) ZnO film. The FFT image shows that the reflections $\{10\bar{1}0\}$ and $\{10\bar{1}1\}$ are observed to be slightly streaked along [1-21-3] direction. This streaking of the diffraction pattern (FFT image) is consistent with the presence of defects, such as basal (0002) stacking faults connected to the unfaulted crystal by partial dislocations, running normal to the [1-21-3] direction. Additional analysis needs to be conducted to determine the rigid body displacement (Burgers vector) of these partial dislocations and if these are intrinsic or extrinsic stacking faults. In addition, there are additional streaked spots on the outermost $\{10\bar{1}1\}$ ring (blue arrows in Figure 4-15b) attributed to pyramidal planes. The additional diffraction spots are indicative of multiple, finer scale grains with local rotation due to the tribological stress/strain-induced sliding process. It is possible in nanocrytalline materials that grain bending/rotation occurs as a result of the POD stress/strain-induced sliding that would give rise to

these new spots (imaging multiple, finer scale grains). The XTEM images support this change wherein the unworn structure has been replaced by a highly disordered structure.

In summary, the ZnO lubricity mechanism is a result of these nanoscale columnar structures being prone to re-orientation during sliding contact. They exhibit new surfaces and subsurfaces which are highly defective. As a result, the ZnO films plastically deform and provide low friction and wear.

CHAPTER 5

CONCLUSIONS

Based on the experimental results, conclusions will be summarized in this chapter. The major goal of this thesis work was to determine the best sputtering conditions to achieve specific film structure which dictates the tribological properties. In general, the best tribological zinc oxide (ZnO) films need some (0002)-orientated grains with a substrate bias voltage to increase the film density. Thus, it was determined that the 200W radio frequency (RF) power, substrate bias -50V at 400C with Nb adhesion layer provided the best overall film. This sputtering recipe was used to deposit the ZnO film on titanium alloys, and the results of pin on disc testing determined that titanium alloys sputtered with ZnO has the lowest friction and highest wear resistance compared to pulsed laser deposition (PLD) and atomic layer deposition (ALD) techniques. In addition, all ZnO films had superior wear resistance compared to the uncoated Ti alloys. In other words, the zinc oxide films improved the wear resistance of titanium alloys, which is a major finding of this thesis.

The ZnO solid lubrication mechanism is a result of the ZnO nanoscale columnar grains being prone to re-orientation during sliding contact. The additional diffraction spots in fast fourier transforms (FFT) images inside the wear track indicated multiple, finer scale grains with local rotation due to the tribological stress/strain-induced sliding process. It is possible in nanocrytalline materials that grain bending/rotation occurs as a result of the pin-on-disc (POD) stress/strain-induced sliding that would give rise to these new spots (imaging multiple, finer scale grains). Thus, inside the wear track there exists new surfaces and subsurfaces which are highly defective. As a result, the ZnO films plastically deform and provide low friction and wear.

This research concludes that it is possible to create low friction and good wear resistance

nanoscale ZnO films by controlling the sputtering parameters which dictate the desired microstructure. The use of the ZnO films should improve the lubricity of titanium alloys in orthopedic implants.

BIBLIOGRAPHY

1. T.C. Niemeyer, C.R. Grandini, L.M.C. Pinto, A.C.D. Angelo, S.G. Schneider, Corrosion behavior of Ti–13Nb–13Zr alloy used as a biomaterial, Journal of Alloys and Compounds 2009; 476:172–175.
2. J.S. Zabinski, J.H Sanders, J Naiparampil and S.V. Prasad, Lubrication using a microstucturally engineered oxide: performance and mechanisms, Tribology Letters 2000; 8:103-116.
3. H. Glieter, Nanocrystalline materials, Progress in Materials Science, 1989; 13:223-315.
4. J. Karch, R. Birringer and H. Glieter, Ceramics ductile at low temperature, Letters to Nature, 1987; 330:556-558.
5. J. Schiotz F.D. Di Tolla and H. Glieterm, Softening of nanocrystalline metals at very small grain sizes, Letters to Nature, 1998; 391:561.
6. Wei Gao, Zhengwei Li, ZnO thin films produced by magnetron sputtering, Ceramics International, 2004; 40:1155-1159.
7. S. Flickyngerova, K. Shtereva, V. Stenova, D. Hasko, I Novotny, V. Tvarizej, P. Sutta, E. Varinsky, Structural and optical properties of sputtered ZnO thin films, Applied Surface Science, 2008; 254:3643-3647.
8. Yuya Kajikawa, Texture development of non-epitaxial polycrystalline ZnO films, Journal of Crystal Growth, 2006; 289:387-394.
9. R. Ondo-Ndong, G. Ferblantier, M. Al Kalfioui, A. Boyer, A. Foucaran, Properties of RF magnetron sputtered zinc oxide thin films, Journal of Crystal Growth, 2003; 255:130-135.
10. J.S. Zabinski, J.H. Sanders, J. Nainaparampil, S.V. Prasad, Lubrication using a

microstructurally engineered oxide, Tribology Letters, 2000; 8:103–116.

11. S.M., Weiderhorn, Brittle Fracture and Toughening Mechanisms in Ceramics, Annu. Rev. Materials Sciences, 1984; 14:373-403.
12. W.M., Rainforth, The wear behavious of oxide ceramics-A Review, Journal of Materials Science, 2004; 39:6705-6721.
13. I.L. Singer, S.D. Dvorak, K.J. Wahl and T.W. Scharf, Role of Third Bodies in Friction and Wear of Protective Coatings, Journal of Vacuum Science and Technology A, 2003; 21(5):232-240.
14. H. Gleiter, Nanocrystalline solids, Journal of Applied Crystal, 1991; 24:79-90.
15. J. Karch, R. Birringer and H. Glieter, Ceramics ductile at low temperature, Letters to Nature, 1987; 330:556-558.
16. J. Schiotz F.D. Di Tolla and H. Glieterm, Softening of nanocrystalline metals at very small grain sizes, Letters to Nature, 1998; 391:561.
17. J.S. Zabinski, J.H Sanders, J Naiparampil and S.V. Prasad, Lubrication using a microstucturally engineered oxide: performance and mechanisms, Tribology Letters 2000; 8:103-116.
18. V.E. Henrich and P.A. Cox, The Surface Science of Metal Oxides, Cambridge University Press, 1994.
19. Ulf. Helmersson, Martina Lattemann, Johan Bohlmark, Arutiun P. Ehiasarian and Jon Tomas Gudmundsson, Ionized physical vapor deposition: review of technology and applications, Thin Solid Films, 2006; 513:1-24.
20. http://www.angstromsciences.com/technology/sputtering-technology/index.html, Sputtering Technology, Angstrom Sciences, Inc.

21. P.J. Kelly, R.D. Arnell, Centre for Advanced Materials and Surface Engineering, Magnetron sputtering: a review of recent developments and applications, Vacuum, 2000; 56:159-172.

22. H R Koenig, L I Maissel, Application of RF discharges to sputtering, IBM Journal of Research and Development, 2000; 44:106-111.

23. G.K. Wehner, Growth of Solid layers on Substrates which are Kept under Ion Bombardment Before and During Deposition, 1962.

24. M. Geetha, A.K. Singh, K. Muraleedharan, A.K. Gogia, R. Asokamani, Effect of thermomechanical processing on microstructure of a Ti-13Nb-13Zr alloy, Journal of Alloys and Compound, 2001; 329:264–271.

25. M. Niinomi, Mechanical properties of biomedical titanium alloys, Materials and Engineering A, 1998; 243:231–236.

26. Sonia Samuel, Soumya Nag, Thomas W. Scharf, Rajarshi Banerjee, Wear resistance of laser-deposited boride reinforced Ti-Nb-Zr-Ta alloy composites for orthopedic implants, Materials Science and Engineering C, 2008; 28:414–420.

27. R. Ondo-Ndonh, G Ferblantier, M. Al Kalfioui, A. Boyer, A. Foucaran, Properties of RF magnetron sputtered zinc oxide thin films, Journal of Crystal Growth, 2003; 255:130-135.

28. Jae-Hyeong Lee, Jun-Tae Song, Dependence of the electrical and optical properties on the bias voltage for ZnO:Al films deposited by r.f. magnetron sputtering, Thin Solid Films, 2008; 516:1377-1381.

29. Wei Gao, Zhengwei Li, ZnO thin films produced by magnetron sputtering, Ceramics International, 2004; 30:1155-1159.

30. W.M. Rainforth, The wear behavior of oxide ceramics-A review, Department of Engineering Materials, Journal of materials science, 2004;39:6705-6721.

31. S. Filckynegerova, K. Shtereva, V. Stenova, D. Hasko, I. Novotny, V. Tvarozek, P. Sutta, E. Vavrinsky, Structural and optical of sputtering ZnO thin films, Applied Surface Science, 2008; 254:3643-3647.

32. Park, S.K., Lee, Y. E., Controlling preferred orientation of ZnO thin films by atomic layer deposition, Journal of Materials Science, 2004; 39:2195-2197.

33. V. E. Henrich and P.A. Cox, The Surface Science of Metal Oxides, Cambridge University Press, 1994.

34. J.S. Zabinski, J. Nainaparampil and S.V. Prasad, Lubrication sing a microstructurally engineered oxide: performance and mechanisms, Tribology letters, 2000; 8:103-116.